doi:10.1093/brain/aws100 Brain 2012: 135; 1794–1818 | 1794

BRAIN
A JOURNAL OF NEUROLOGY

Limiting multiple sclerosis related axonopathy by blocking Nogo receptor and CRMP-2 phosphorylation

Steven Petratos,[1,2,*] Ezgi Ozturk,[1,*] Michael F. Azari,[1] Rachel Kenny,[1] Jae Young Lee,[1] Kylie A. Magee,[1] Alan R. Harvey,[3] Courtney McDonald,[1] Kasra Taghian,[2] Leon Moussa,[1] Pei Mun Aui,[1] Christopher Siatskas,[1] Sara Litwak,[1] Michael G. Fehlings,[4,5,6] Stephen M. Strittmatter[7] and Claude C. A. Bernard[1]

1 Monash Immunology and Stem Cell Laboratories, Monash University, Clayton Victoria 3800, Australia
2 Molecular Neuropathology and Experimental Neurology Laboratory, School of Medical Sciences and Health Innovations Research Institute, Royal Melbourne Institute of Technology University, Bundoora Victoria 3083, Australia
3 School of Anatomy, Physiology and Human Biology, The University of Western Australia, Crawley Western Australia 6009, Australia
4 University of Toronto Neuroscience Program, Toronto, Canada
5 McEwen Centre for Regenerative Medicine, Toronto, Canada
6 Toronto Western Research Institute, Krembil Neuroscience Centre, Toronto, Canada
7 Program in Cellular Neuroscience, Neurodegeneration and Repair, Yale University School of Medicine, New Haven, CT 06536, USA

*These authors contributed equally to this work.

Correspondence to: Dr Steven Petratos,
Monash Immunology and Stem Cell Laboratories,
Monash University,
Clayton VIC 3800, Australia
E-mail: steven.petratos@monash.edu

Multiple sclerosis involves demyelination and axonal degeneration of the central nervous system. The molecular mechanisms of axonal degeneration are relatively unexplored in both multiple sclerosis and its mouse model, experimental autoimmune encephalomyelitis. We previously reported that targeting the axonal growth inhibitor, Nogo-A, may protect against neurodegeneration in experimental autoimmune encephalomyelitis; however, the mechanism by which this occurs is unclear. We now show that the collapsin response mediator protein 2 (CRMP-2), an important tubulin-associated protein that regulates axonal growth, is phosphorylated and hence inhibited during the progression of experimental autoimmune encephalomyelitis in degenerating axons. The phosphorylated form of CRMP-2 (pThr555CRMP-2) is localized to spinal cord neurons and axons in chronic-active multiple sclerosis lesions. Specifically, pThr555CRMP-2 is implicated to be Nogo-66 receptor 1 (NgR1)-dependent, since myelin oligodendrocyte glycoprotein $(MOG)_{35–55}$-induced NgR1 knock-out ($ngr1^{-/-}$) mice display a reduced experimental autoimmune encephalomyelitis disease progression, without a deregulation of $ngr1^{-/-}$ $MOG_{35–55}$-reactive lymphocytes and monocytes. The limitation of axonal degeneration/loss in experimental autoimmune encephalomyelitis-induced $ngr1^{-/-}$ mice is associated with lower levels of pThr555CRMP-2 in the spinal cord and optic nerve during experimental autoimmune encephalomyelitis. Furthermore, transduction of retinal ganglion cells with an adeno-associated viral vector encoding a site-specific mutant T555ACRMP-2 construct, limits optic nerve axonal degeneration occurring at peak stage of experimental autoimmune encephalomyelitis. Therapeutic administration of the anti-Nogo(623–640) antibody during the course of experimental autoimmune encephalomyelitis, associated with an improved clinical outcome, is demonstrated to abrogate the protein levels of pThr555CRMP-2 in the spinal cord and improve pathological outcome. We conclude that phosphorylation of CRMP-2 may

Received August 19, 2011. Revised March 7, 2012. Accepted March 7, 2012. Advance Access publication April 28, 2012

be downstream of NgR1 activation and play a role in axonal degeneration in experimental autoimmune encephalomyelitis and multiple sclerosis. Blockade of Nogo-A/NgR1 interaction may serve as a viable therapeutic target in multiple sclerosis.

Keywords: Nogo receptor; Nogo-A; collapsin response mediator protein 2; experimental autoimmune encephalomyelitis; axonal degeneration

Abbreviations: DAPI = 4′,6-diamidino-2-phenylindole; EAE = experimental autoimmune encephalomyelitis; GFP = green fluorescent protein; MOG = myelin oligodendrocyte glycoprotein; rAAV2 = recombinant adeno-associated virus 2

Introduction

Multiple sclerosis is a severe neurological disorder that involves inflammation in the brain and spinal cord, axonal damage and demyelination. Experimental autoimmune encephalomyelitis (EAE) is an animal model that mimics many of the pathophysiological hallmarks of multiple sclerosis. The induction of EAE by immunization with the myelin oligodendrocyte glycoprotein (MOG) peptide encompassing the 35–55 amino acid sequence ($MOG_{35–55}$) is a commonly used animal model for the neurodegenerative changes observed in multiple sclerosis (Johns *et al*., 1995). It has long been believed that axonal damage, degeneration and loss are secondary to demyelination. However, data from our laboratory have demonstrated that axonal degeneration can precede demyelination in EAE (Wang *et al*., 2005). Notably, Trapp *et al*. (1998) have reported the appearance of newly transected axons in active and hypocellular chronic-active multiple sclerosis lesions from brains obtained at autopsy, suggesting a relationship between axonal damage and permanent neurological deficits.

It is likely that multiple sclerosis may display similar pathogenic mechanisms and features as observed in spinal cord injury, whereby degenerating axons may attempt regeneration, but fail due to the inhibitory environmental cues (Jurewicz *et al*., 2007). The factors in the adult CNS that inhibit these compensatory regenerative responses include myelin proteins and extracellular matrix constituents (Profyris *et al*., 2004). Chief among these factors are integral components of myelin known as the myelin-associated inhibitory factors, such as the potent inhibitor of neurite outgrowth, Nogo-A (GrandPre *et al*., 2000; Fournier *et al*., 2001). Expression of Nogo-A in oligodendrocytes has been reported to be upregulated in active demyelinating lesions of multiple sclerosis (Satoh *et al*., 2005). In addition, our laboratory has demonstrated that immunization against Nogo-A or deletion of the *nogo* gene ameliorates the effects of EAE (Karnezis *et al*., 2004). While Nogo-A is known to be a potent inhibitor of axonal regrowth, a direct relationship with *bona fide* axonal pathology, an important feature of both EAE and multiple sclerosis lesions (Trapp *et al*., 1998; Wang *et al*., 2005), is as yet undefined. Although recent evidence has demonstrated that deletion of the co-receptor for Nogo-A, LINGO-1, improves axonal integrity and protects against neurological decline in MOG-induced EAE (Mi *et al*., 2007), the mechanism by which this eventuates is not known. Furthermore, small interfering RNA silencing of Nogo-A in both $MOG_{35–55}$- and myelin basic protein-induced EAE models has been shown to limit the clinical severity of the disease and promote repair (Yang *et al*., 2010) but again it is unclear how this therapeutic effect is achieved. This raises the question of whether in EAE and multiple sclerosis, Nogo-A can signal axonal degeneration through its axonally localized cognate receptors.

In this study, we show for the first time that phosphorylated collapsin response mediator protein 2 (CRMP-2) (pThr555CRMP-2, a key molecule that regulates microtubule assembly) is abundant in degenerating spinal cord neurons and their axons of EAE-induced mice and active multiple sclerosis lesions. We are able to define further that the increase in axonally specific pThr555CRMP-2 is limited in EAE-induced *ngr1*$^{-/-}$ mice, thereby preventing significant axonal and myelin degeneration characteristic of $MOG_{35–55}$ EAE. Moreover, the introduction of a site-specific T555A mutation in CRMP-2 through a recombinant adeno-associated virus 2 (rAAV2) delivery system to retinal ganglion cells, limits axonal degeneration in the optic nerve during the peak stage of EAE. Finally, we highlight the contribution of pThr555CRMP-2 during the neurodegenerative phase of EAE by reducing the spinal cord levels and associated axonal pathology through the passive transfer of anti-Nogo-A antibodies. Thus, reducing the NgR1-dependent signalling capacity during EAE may limit the activation of the phosphorylation of CRMP-2, thereby preventing axonal degeneration and neurological decline. By extension, these data advocate for targeting NgR1 signalling in multiple sclerosis.

Materials and methods

Animals, induction of $MOG_{35–55}$ EAE and analysis of clinical progression

Female C57Bl/6 mice (aged 10 – 16 weeks) were bred and maintained at Monash University Animal House. Experiments were performed in accordance with the Australian code of practice for the care and use of animals for scientific purposes, approved by the Monash University Animal Ethics Committee and Office of the Gene Technology Regulator of Australia. The *ngr1* exon 2 gene mutation is a doubly targeted allele on a C57Bl/6 background and backcrossed more than eight generations as previously described (Kim *et al*., 2004). To induce EAE, a total of 200 μg of the encephalitogenic peptide, $MOG_{35–55}$ (GenScript) emulsified in 200 μl of complete Freund's Adjuvant (Sigma-Aldrich), supplemented with 4 μg/ml *Mycobacterium tuberculosis* was injected subcutaneously into the lower flanks, then followed with an intraperitoneal injection of 350 ng pertussis toxin (Sigma-Aldrich). Mice were injected with a second dose of pertussis toxin 48 h later (Karnezis *et al*., 2004). Female *ngr1*$^{-/-}$ ($n = 22$) and *ngr1*$^{+/+}$ ($n = 14$) mice were graded daily post-$MOG_{35–55}$ injection (days post-injection) for disease progression (Bernard *et al*., 1997) corresponding to pre-onset (7 days post-injection),

onset (12 days post-injection), peak (18 days post-injection) and chronic (30 days post-injection) stages of disease (in wild-type C57Bl/6 mice, $n = 53$), respectively. Severely paralysed mice (Score 3–4) were killed with CO_2 inhalation; serum and tissues were then collected. The brain (including optic nerves) and spinal cord were removed and immediately snap frozen in tubes using liquid nitrogen. For histological experiments, the animals were initially transcardially perfused with 0.1 M phosphate-buffered saline (pH 7.4), followed with 4% paraformaldehyde. The tissue was dehydrated in 30% sucrose for 48 h. For toluidine blue staining and microscopy, animals were processed with 2.5% gluteraldehyde and 4% paraformaldehyde as previously described (Azari *et al*., 2006).

Human post-mortem brain and spinal cord tissue

Human CNS tissue was obtained through the Department of Anatomical Pathology, The Royal Melbourne Hospital, in accordance with the National Health and Medical Research Council guidelines and the Monash University Human Research Ethics Committee for the use of human specimens in medical research. Post-mortem delay did not exceed 24 h and biopsy delay was <1 h. The following tissues were used in the current study (Table 1). Multiple sclerosis cases: four secondary progressive (67 plaques analysed from brain and spinal cord), three hyperacute (three plaques analysed from brain); other neurological diseases: epilepsy (one case from temporal lobe), progressive multifocal leukoencephalopathy (three cases from brain), Alzheimer's disease (two cases from frontal lobe), meningitis (one case from frontal lobe); non-neurological diseases: death by natural causes (10 cases from brain). Brain tissues were immersion fixed in 10% buffered formalin and paraffin embedded, then cut at 10 μm using a conventional microtome and mounted on Superfrost Plus® slides (Menzel-Gläser). Histological analysis of de-waxed human CNS tissue was performed as described below.

Histopathology: inflammation, demyelination and axonal degeneration/loss

Histological evaluation was performed on 4% paraformaldehyde-fixed, O.C.T-embedded 10-μm sections of cerebellum, optic nerve and spinal cord. Sections were stained using Luxol fast blue and Periodic acid Schiff (to demonstrate demyelination and inflammatory cell infiltration, respectively) and Bielschowsky silver stains (to demonstrate axonal degeneration/loss), as described previously (McQualter *et al*., 2001). A trained histopathologist semi-quantitatively scored more than three sections per mouse, per genotype or per antibody-treated group [see anti-Nogo(623–640) antibody treatment section below] in a blinded manner. The following criteria were used to define histopathological inflammation and demyelination events respectively: 0, no inflammation; 1, cellular infiltrate only in the perivascular areas and meninges; 2, mild cellular infiltrate in parenchyma; 3, moderate cellular infiltrate in parenchyma; and 4, severe cellular infiltrate in parenchyma. The myelin breakdown was assessed by pale staining with Luxol fast blue (no evidence of remyelination) and scored in a blind fashion as follows: 0, no demyelination; 1, mild demyelination; 2, moderate demyelination and 3, severe demyelination. Images were captured in bright-field under a UPlanApo $\times 40$ 1.20 NA objective lens of an Olympus Provis A $\times 70$ microscope. The captured 16-bit images were then converted to TIFF files and the images were assembled and formatted using Adobe Photoshop vCS3 software.

Antibodies and reagents

The following primary antibodies were used: rabbit polyclonal anti-pThr555CRMP-2 affinity purified (generated by the authors), mouse monoclonal anti-CRMP-2 affinity purified clone (Immuno-Biological Laboratories Co. Ltd.), rabbit polyclonal anti-pThr514CRMP-2 (Cell Signaling Technology), mouse monoclonal anti-tau-5 (Calbiochem), mouse monoclonal anti-hyperphosphorylated-tau (clone AT8; Pierce-Thermo Scientific), rabbit polyclonal anti-pSer199/202-tau (Biosource), mouse monoclonal anti-NF200 (Sigma-Aldrich), mouse monoclonal anti-βIII-tubulin (clone Tuj-1; Millipore-Chemicon), rat monoclonal anti-α-tubulin (Millipore-Chemicon), mouse monoclonal anti-β-actin (Sigma-Aldrich), mouse anti-human CD3 (BD Pharmingen). The following secondary antibodies were used: sheep polyclonal anti-mouse horseradish peroxidase (HRP)-conjugated affinity purified IgG, goat polyclonal anti-rabbit HRP-conjugated affinity purified IgG, goat polyclonal anti-mouse Alexa Fluor® 555 affinity purified IgG, goat polyclonal anti-rabbit Alexa Fluor® 488 affinity purified IgG (Molecular

Table 1 Tissue collected from patients with multiple sclerosis[a]

Patient No.	Sex	Age (years)	Histopathological assessment	Duration of disease	Tissue location	No. of blocks taken at autopsy	No. of active plaques	*PThr555CRMP2* + immunopositivity			
								Total No. of positive plaques	Plaque core	Periplaque	Grey matter
1	F	38	Chronic-active MS	11 years	1–14	18	13	13	7	6	4
2	F	44	Chronic-active MS	8 years	1, 3, 4, 8–14	16	13	13	5	5	6
3	F	37	Chronic-active MS	12 years	1, 3, 4, 8–14	16	13	13	6	9	8
4	M	52	Chronic-active MS	7 years	1, 3, 4, 6	14	13	13	4	8	4
5	F	51	Active MS	4 months	3	1	1	1	1	1	0
6	M	25	Hyperactive MS	9 months	1	1	1	1	1	1	0
7	F	40	Hyperactive MS	10 weeks	1	1	1	1	1	1	0

a Post-mortem delay <24 h; biopsy delay <1 h.
MS = multiple sclerosis; 1 = frontal lobe white matter; 2 = periventricular white matter, including subventricular zone of the anterior horn of the lateral ventricle; 3 = internal capsule including striatum; 4 = temporal lobe deep white matter; 5 = occipital lobe deep white matter; 6 = cerebellum; 7 = midbrain; 8 = rostral pons; 9 = caudal pons; 10 = rostral medulla; 11 = caudal medulla; 12 = cervical cord; 13 = thoracic cord; 14 = lumbar cord.
As demonstrated by Luxol fast blue/periodic acid Schiff staining, as well as CD68- and CD3-immunostaining.

Probes). For immunoprecipitation experiments, the control peptides included full-length CRMP-2 and the pThr555CRMP-2 peptide (Millipore).

Production of anti-pThr555CRMP-2 polyclonal antibody

A rabbit polyclonal antibody was generated against the pThr555CRMP-2 peptide sequence [Cys-Ile550-Pro-Arg-Arg-Thr-Thr(P)-Gln-Arg-Ile-Val-Ala560] as previously reported (Arimura *et al*., 2000). Characterization of anti-pThr555CRMP-2 antibody was by enzyme-linked immunosorbent assay, demonstrating phospho-peptide reactivity with the affinity purified polyclonal antibody. Immunoreactivity was at 1:10 000 dilution of the anti-pThr555CRMP-2 antibody using 5 μg of the pThr555CRMP-2 peptide (Millipore) as substrate. Mouse spinal cord lysates reacted with the anti-pThr555CRMP-2 antibody by western blot showing a 62 kDa band, which was subsequently demonstrated to be CRMP-2 by mass spectrometry. The 62 kDa band immunoreactivity was blocked by preincubation of the antibody with the pThr555CRMP-2 peptide (20 μg). Preincubation with the same CRMP-2 peptide without phosphorylation produced the same immunoreactive 62 kDa band demonstrating the phospho-specificity of the antibody. Incubation with the pre-bleed antiserum showed no reactivity with the 62 kDa band.

Preparation of tissue lysates for western blotting

Spinal cord and optic nerve tissues were ground and lysed using RIPA buffer with protease inhibitor (Sigma-Aldrich) and PhosSTOP™ phosphatase inhibitor cocktail (Roche Applied Science) in a dounce homogenizer. Homogenates were centrifuged at 13 000 × *g* for 20 min and protein concentrations of the supernatants determined using the bicinchoninic acid protein assay reagent kit (Pierce) as previously described (Petratos *et al*., 2008).

Amyloid-β treated human SH-SY5Y neuroblastoma cell culture, Tg2576 transgenic animals and Alzheimer's disease brain tissue

SH-SY5Y cells were cultured and differentiated with retinoic acid as previously described (Petratos *et al*., 2008). Cells were treated with the 10 μM amyloid-β peptide diluted in Dulbecco's modified Eagle medium: nutrient mixture F-12 (Invitrogen) for 24 h. The cells were then lysed using cell lysis buffer and then run on a 12% sodium dodecyl sulphate polyacrylamide gel. Transgenic Tg2576 female mice at 18 months of age, along with human Alzheimer's disease frontotemporal brain tissue were used as positive controls for the tau phosphorylation and hyperphosphorylation western blot studies. Sarcosyl-insoluble tau preparations were prepared as previously described (Anderson *et al*., 2008).

Western immunoblotting

We loaded and ran 5 μg of protein on a 4–12% graded sodium dodecyl sulphate polyacrylamide gel (Invitrogen). Proteins were then electrophoretically transferred onto polyvinylidene fluoride membranes (Millipore). The membranes were blocked with 5% skimmed milk powder and the primary antibodies diluted in this blocking buffer (polyclonal anti-pThr555CRMP-2, 1:1000; monoclonal anti-CRMP-2, 1:1000; anti-α-tubulin, 1:1000; anti-β-actin, 1:5000; anti-pThr514CRMP-2, 1:1000; anti-tau5, 1:1000) were incubated overnight at 4°C. After washing the membranes in 0.1% v/v Tris-buffered saline-Tween, the secondary anti-rabbit (1:1000), anti-sheep (1:1000), anti-mouse (1:1000) or anti-rat (1:1000) HRP-conjugated antibodies were incubated for 2 h at room temperature. Immunoreactive proteins were detected using an ECL Plus™ chemiluminescence method (Amersham). The level of immunostaining was determined by image analysis after scanning the exposed films using AlphaImager® (Alpha Innotech) and then processing the 16-bit monochrome images through the ImageQuant TL™ v2003 software (Nonlinear Dynamics, Ltd.) to measure pixel intensity relative to background. The level of staining was normalized with β-actin or α-tubulin and expressed as arbitrary units. Percentages of band levels were also derived by setting the controls as 100% and the test samples were determined to be elevated or reduced from this basal level. All protein bands were analysed from at least four separate samples and statistics then performed (as described below).

Immunoprecipitation

To measure the level of total CRMP-2 or α-tubulin prior to immunoprecipitation of CRMP-2, 5% of the starting amount was run on a 4–12% graded sodium dodecyl sulphate polyacrylamide gel. All immunoprecipitation assays were performed from samples containing 100 μg of total protein in 1 ml of lysate buffer. Immunoprecipitation was performed by adding 2 μg of polyclonal anti-pThr555CRMP-2 or monoclonal anti-CRMP-2 (IBL) capture antibody to each sample. Rabbit IgG or mouse IgG was used as negative controls and the positive control included pThr555CRMP-2 peptide with the anti-pThr555CRMP-2 antibody. Samples were incubated overnight at 4°C followed by the addition of 70 μl of a 50% slurry of Protein A-Sepharose beads (Millipore) for incubations with polyclonal anti-pThr555CRMP-2 antibody or 70 μl of 50% Protein G Sepharose beads (Millipore) for incubations with monoclonal anti-CRMP-2 antibody. The immunoprecipitation and co-immunoprecipitation procedures were then performed as previously described (Petratos *et al*., 2008) and samples were loaded onto a 4–12% sodium dodecyl sulphate-polyacrylamide gel and then transferred onto a polyvinylidene fluoride membrane for immunoblotting.

Sarcosyl gradient centrifugation

Sarcosyl-insoluble tau preparation was done as previously described (Anderson *et al*., 2008). Briefly, lumbosacral spinal cords were homogenized in a 10× volume of high salt buffer of 10 mM Tris (pH 7.4), 0.8 M sodium chloride, 1 mM EGTA, 10% sucrose (w/v). The extracts were centrifuged at 45 000*g* for 30 min, supernatants collected and pooled, then subjected to another extraction with a 5× volume of the same buffer. The pooled supernatant fraction was incubated with 1% sarcosyl for 1 h then centrifuged at 260 000*g* for 1 h at 4°C. The resulting pellet represented the sarcosyl insoluble tau preparation.

Immunofluorescence

Mouse cryostat sections

Following transcardial perfusion of the mice with 4% paraformaldehyde, the lumbar enlargements of the spinal cords were removed and embedded in O.C.T (Tissue-Tek® Sakura Finetek Inc.). Serial 10-μm

thick longitudinal sections were then cut on a cryostat (CM 1900, Leica Microsystems) and mounted on Superfrost Plus® slides (Menzel-Gläser). The tissue was initially incubated with blocking buffer (phosphate-buffered saline supplemented with 3% goat serum, 3% mouse serum and 0.3% Triton X-100) for 2 h at room temperature. The sections were incubated with primary antibodies in blocking buffer overnight at 4°C. The samples were washed three times in phosphate-buffered saline (pH 7.4) for 10 min, followed by 2-h incubation with secondary antibodies (goat anti-mouse Alexa Fluor® 488, goat anti-rabbit Alexa Fluor® 555; Invitrogen) at room temperature. After three washes with phosphate-buffered saline, the sections were stained with 4′,6-diamidino-2-phenylindole (DAPI; Molecular Probes) for 10 min, washed and cover-slipped using fluorescent mounting medium (Dako). Primary antibodies used were mouse anti-βIII-tubulin (1:500), mouse anti-NF200 (1:200) and rabbit anti-pThr555CRMP-2 (1:200). Images were captured by fluorescence with an UPlanApo ×40 1.20 NA objective lens of an Olympus Provis Ax70 microscope.

Human tissue

Sections were microwaved for antigen retrieval (two 5 min washes in 0.1 M citrate buffer, pH 6), thoroughly washed (three 10 min washes in phosphate-buffered saline, pH 7.4) and incubated with proteinase K (20 μg/ml, 1 h at 37°C). Following further phosphate-buffered saline washes and post-fixation with 4% paraformaldehyde (30 min at room temperature), the sections were incubated with blocking buffer (10% foetal calf serum and 0.3% Triton X-100 in phosphate-buffered saline) overnight at 4°C. Human CNS tissues were then incubated with primary antibodies [mouse anti-NF200 (1:200), mouse anti-AT8 (1:50); mouse anti-human CD3 (1:50); rabbit anti-pThr555CRMP-2 (1:200)] for 48 h at 4°C then followed by secondary anti-mouse (Alexa Fluor® 488) and anti-rabbit (Alexa Fluor® 555), diluted at 1:200, incubated with DAPI, mounted with fluorescent mounting medium and cover-slipped. All human tissue specimens were captured by three channel fluorescence imaging using a confocal Leica TCS NT upright or inverted microscope with the following objective lenses: UPlanApo ×20 0.75 NA, ×40 1.20 NA or ×60 1.40 NA. The captured 16-bit images were then converted to TIFF files and the images were assembled and formatted using Adobe Photoshop vCS3 software.

Analysis of demyelination and axonal calibre

Mice perfused with 2.5% gluteraldehyde and 4% paraformaldehyde were dissected and the optic nerves and lumbosacral spinal cords post-fixed. Optic nerves were embedded in resin and prepared for ultrastructural analysis of demyelination by calculating *G*-ratios as previously described (Azari *et al*., 2006). Toluidine blue staining was performed and photomicrographs were then obtained from these regions using a light dotSlide™ BX51 microscope (Olympus) with a digital camera (2.3.0, RT Slider, Diagnostic Instruments, Inc.). Thickness of axons and their surrounding myelin were measured using the MetaMorph® software. At least 300 axons were measured from serial sections ($n = 3$ sections per animal and $n = 3$ animals per group) at a distance of 100 μm apart, with values expressed as mean ± SEM. Percentage of demyelination in the optic nerve was calculated from the *G*-ratio data by converting the basal level of the mean ratio in the adjuvant injected *ngr1*$^{+/+}$ control to 100%, then converting the EAE-induced mouse optic nerve ratios to a percentage relative to that basal level (Azari *et al*., 2006).

Adeno-associated virus 2 construction and production

The construction of rAAV2-Flag-CRMP2T555A-GFP and control rAAV2-GFP plasmids was generated through Vector BioLabs. Briefly, site-directed mutagenesis was performed on complementary DNA of human CRMP-2 (a gift from Professor Christina Mitchell, Monash University) as previously described (Arimura *et al*., 2000) using the Stratagene Quikchange® kit (Agilent Technologies) and subloned in the pRK-5-Flag vector. The Flag-CRMP2T555A complementary DNA was subcloned into the pAAV cis-plasmid, with green fluorescent protein (GFP) co-expression. An endotoxin-free, mega-prep of the pAAV cis-plasmid was then followed by transient co-transfection of the cis-plasmid with Ad Helper and RepCap plasmids into 10 plates (150 cm) of 293 cells to demonstrate the fidelity of the plasmid vector. Purification of the rAAV was completed through two rounds of CsCl centrifugation and viral titres (measuring genomic copies, i.e. intact virus) were accomplished rendering 2.1×10^{13} genomic copies/ml for rAAV2-Flag-CRMP2T555A-GFP and 1.0×10^{13} genomic copies/ml for rAAV2-GFP.

Surgery, intraocular injections and tissue processing

Female C57Bl/6 mice (aged 10 weeks) were anaesthetized by intraperitoneal injection of 2% xylazine (7 mg/kg body weight) and 10% ketamine (95 mg/kg body weight). Using a finely pulled micropipette, the left eyes of mice were injected from the temporal quadrant with 1.5 μl of either the rAAV2-GFP or the rAAV2-Flag-CRMP2T555A-GFP ($n = 8$ per virally injected group, total viral particles injected per eye were 0.75×10^{10}), directly into the vitreous (Leaver *et al*., 2006; Hellstrom and Harvey, 2011). Following AAV injection, all mice were left for 7 days then immunized with $MOG_{35–55}$ and pertussis toxin as described above, to induce EAE. A separate group of mice ($n = 5$), not injected with AAV, were also EAE-induced as a control group. The mice were then left to progress clinically to peak stage of disease, which did not exceed clinical score 3 and/or Day 22 post-EAE induction.

All mice (including uninjected control EAE-induced mice) were then perfusion fixed with 4% paraformaldehyde and the optic nerves and retinae collected for immunohistochemistry and axonal counts. Briefly, optic nerves were post-fixed in 4% paraformaldehyde for 24 h and eyes for 3 days at 4°C, then both tissues placed in 20% sucrose overnight. Retinae were dissected from eyes and incubated as free-floating tissue with Alexa Fluor® 488 conjugated rabbit anti-GFP (1:200 dilution, Molecular Probes) in blocking buffer and mouse anti-βIII tubulin antibody (1:2000) according to immunofluorescence protocols defined above. Optic nerves were paraffin embedded, then 14 μm serial longitudinal sections cut on a microtome, collecting every section. Three sections per optic nerve, at least 28 μm apart, were immunostained using goat anti-GFP biotinylated antibody (1:200) then followed with either streptavidin conjugated with Alexa Fluor® 488, mouse anti-Flag antibody (1:200), rabbit anti-pThr555CRMP-2 antibody (1:500) or mouse anti-amyloid precursor protein antibody (1:500, Merck-Millipore). Secondary antibodies consisted of either goat anti-mouse Alexa Fluor® 488 or goat anti-rabbit Alexa Fluor® 555 and the optic nerve sections were processed as defined for immunofluorescence above.

Axonal degeneration was defined according to morphological abnormalities in rAAV2-tranduced, GFP-positive axons. GFP-positive clearly transected axons with retraction bulbs/spheroids were

expressed as a percentage of the total number of GFP-positive axons per square millimetre of the left optic nerve.

Therapeutic anti-Nogo(623-640) antibody treatment of EAE-induced mice

Anti-Nogo(623–640) affinity purified antibody was generated as previously described (Karnezis *et al*., 2004) and concentrated at 1 mg in 0.2 ml for *in vivo* use. Three intravenous administrations of this antibody at Days 8, 11 and 14, and two intraperitoneal injections on Days 9 and 16 were performed in post-$MOG_{35–55}$ EAE-induction in adult C57Bl/6 mice ($n = 4$). A control administration of non-specific affinity purified rabbit IgG was also performed at the same time-points and routes of administration ($n = 4$) as the anti-Nogo(623–640) antibody-treated group. Another group received no antibody administration ($n = 4$). Clinical progression data are expressed as mean ± SEM.

Statistics

Data were analysed using Graph Pad Prism v3.02 software. A one-tailed Student's *t*-test or a one-way ANOVA with Tukey's *post hoc* test was used to determine statistical significance ($P < 0.05$) at a 95% confidence level for optical density levels obtained from immunoblot analysis. Friedman's non-parametric repeated measures and Dunn's multiple-comparison were used for analysis of differences in the clinical progression of EAE between different genotypes, rAAV-injected or different antibody treatment groups of mice.

Results

Phosphorylation of CRMP-2 correlates with axonal degeneration in EAE

The progression of axonal degeneration and demyelination (Supplementary Fig. 1B) directly correlates with the extant motor deficit in C57Bl/6 female mice after induction of $MOG_{35–55}$-EAE (Supplementary Fig. 1A). During the most disabling time-points of EAE (by Days 18 and 30, characterized as peak and chronic forms of the disease respectively; Supplementary Fig. 1A), the greatest levels of inflammation (score of 2.5 ± 0.26 for peak, 2.75 ± 0.43 for chronic, in the lumbosacral spinal cord; Supplementary Table 1), demyelination (score of 1.25 ± 0.22 for peak, 2.0 ± 0.37 for chronic in the lumbosacral spinal cord; Supplementary Table 1) and axonal degeneration/loss (Supplementary Fig. 1B) were demonstrated. Since the molecular mechanism(s) involved in axonal degeneration following spinal cord injury has been shown to involve an increase in CRMP-2 phosphorylation (Mimura *et al*., 2006), we investigated the levels of phosphorylated CRMP-2 during EAE-dependent axonal degeneration (Fig. 1). Following EAE induction, there was an incremental increase of pThr555CRMP-2B in spinal cord lysates when compared with adjuvant-injected controls (Fig. 1A and C). Intriguingly, there was also an increase in the level of the pThr555 N-terminal variant of CRMP-2, i.e. CRMP-2A, in EAE-induced mice that could not be demonstrated in the adjuvant injected controls (Fig. 1C).

Phosphorylated CRMP-2 was localized to axons around inflammatory lesions within spinal cord sections of EAE-induced mice, using the polyclonal pThr555CRMP-2 antibody (Fig. 1E). There were increased levels of pThr555CRMP-2 immunofluorescence co-localized with βIII-tubulin-labelled degenerative axons near inflammatory lesions (Fig. 1E).

Localization of pThr555CRMP-2 in degenerating neuronal somata and axons of acute and chronic-active multiple sclerosis lesions

Given that increased levels of pThr555CRMP-2 could be demonstrated in EAE mice particularly at peak of disease, we next assessed whether this specific phosphorylation event could also be demonstrated in human active demyelination and axonal degeneration as pathologically depicted in patients with multiple sclerosis. We obtained brain and spinal cord paraffin-embedded tissue samples from four chronic-active and three acute-active multiple sclerosis autopsy cases (Table 1). As shown in Fig. 2A, demyelination along with axonal degeneration (Fig. 2B and C) was apparent in the dorsolateral tracts of the lumbar spinal cord. Degenerating ventral horn motor neurons (Fig. 2D and E) were also demonstrable near inflammatory perivenular lesions in the grey matter (Fig. 2F). In acute-active demyelinating brain lesions, there were numerous tissue areas of active macrophage phagocytosis of myelin (Supplementary Fig. 2A) with extracellular myelin debris and axonal damage (Supplementary Fig. 2B). All of the active multiple sclerosis lesions were immunopositive for pThr555CRMP-2 in the brain and spinal cord (Table 1). In contrast, pThr555CRMP-2 immunoreactivity could not be demonstrated in non-neurological disease control samples or most brain samples with other neurological diseases, including demyelinating disease from progressive multifocal leukoencephalopathy specimens (Table 2). We did, however, detect immunopositivity for pThr555CRMP-2 in cerebral cortex and subcortical white matter from a sample that was collected at post-mortem with meningitis along with chronic neurodegeneration of two patients with Alzheimer's disease. The rationale for including Alzheimer's disease brain tissue in this study derives from the fact that hyperphosphorylation of CRMP-2 has been previously reported in brain tissue from patients with Alzheimer's disease and specifically localized to neurofibrillary tangles (Yoshida *et al*., 1998; Gu *et al*., 2000; Cole *et al*., 2007; Takata *et al*., 2009; Williamson *et al*., 2011). Furthermore, we have reported that small molecular weight amyloid-β species can potentiate the phosphorylation of CRMP-2 at the Thr555 site in human SH-SY5Y cells (Petratos *et al*., 2008).

Acute and chronic-active demyelinated multiple sclerosis lesions in the brain and spinal cord all showed pThr555CRMP-2 positive axonal staining in the plaque core and periplaque white matter (Table 1). No pThr555CRMP-2 immunostaining was detected in chronic-inactive plaques, which showed a lack of macrophage/microglial activity with a sharp lesion border (Table 1). Subsets of grey matter NF200-positive neurons and axons present in the lumbar spinal cord from individuals with chronic-active multiple

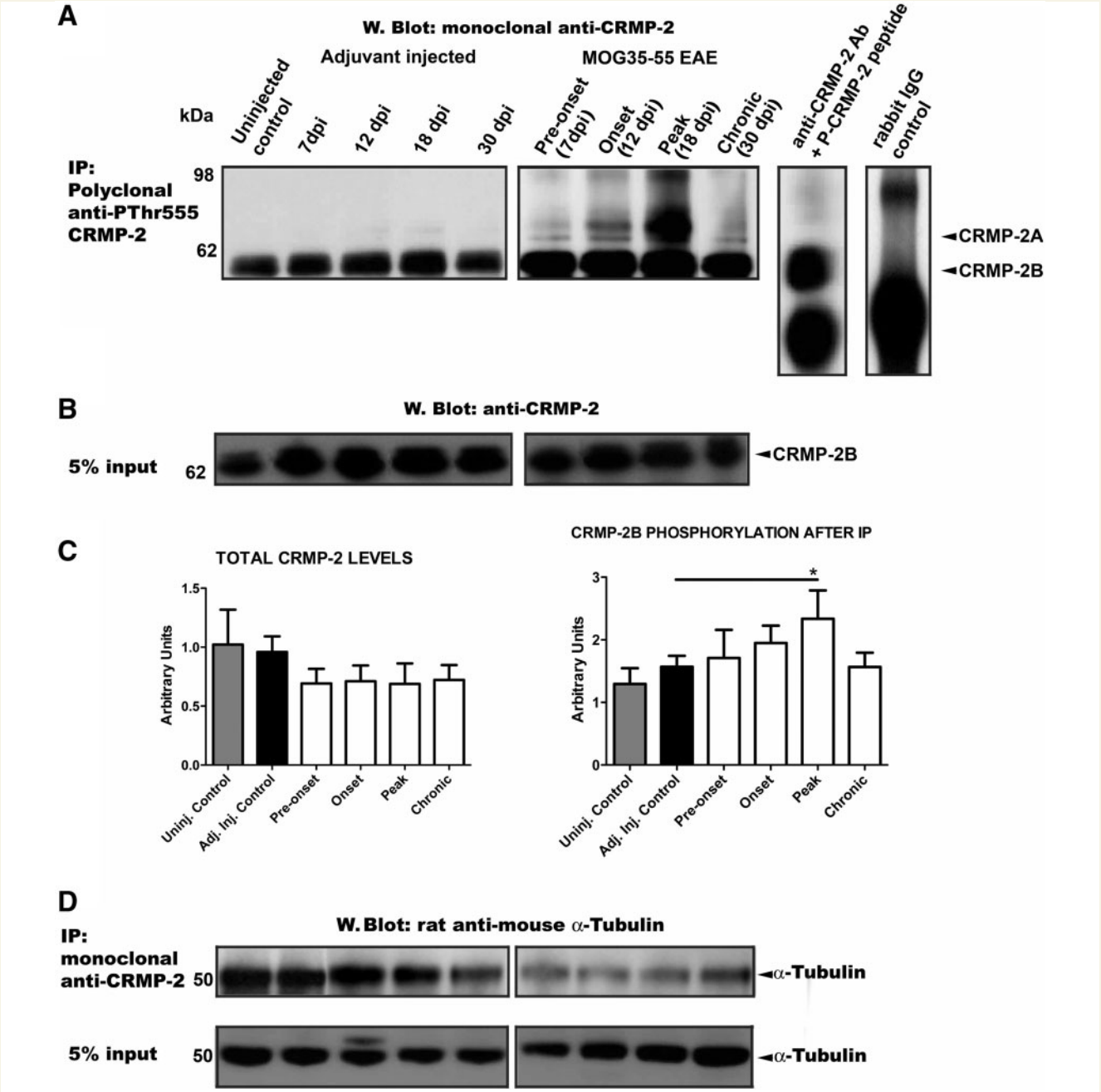

Figure 1 Phosphorylation of CRMP-2 correlates with axonal degeneration in EAE. (**A**) Immunoprecipitation of pThr555 CRMP-2 using our polyclonal anti-pThr555 CRMP-2 antibody, of lumbosacral spinal cord lysates, dissected from wild-type MOG_{35-55}-induced EAE, uninjected control or adjuvant injected alone control mice, followed by western immunoblot analysis using the monoclonal anti-CRMP-2 antibody. Control wells include non-specific rabbit IgG polyclonal antibody and pThr555 CRMP-2 (20 μg) peptide spiked in lysate buffer alone. The membranes were then reprobed using the monoclonal anti-CRMP-2 antibody. (**B**) Western immunoblot for CRMP-2 from spinal cord lysate samples loaded pre-immunoprecipitation (5% input of immunoprecipitation sample) using the monoclonal anti-CRMP-2 antibody. (**C**) Densitometric quantification (AU) of total CRMP-2 and pThr555 CRMP-2B (after immunoprecipitation) from spinal cord lysates of control and EAE-induced mice ($n = 4$ mice per group and per time-point; $^*P < 0.05$ one-way ANOVA). (**D**) Co-immunoprecipitation of CRMP-2-associated tubulin was performed from control and EAE-induced spinal cord lysates using monoclonal anti-CRMP-2 antibody followed by western immunoblotting with rat anti-mouse α-tubulin. Total loading levels of tubulin for each spinal cord sample pre-immunoprecipitation were demonstrated by loading 5% input of total protein (from the same samples illustrated in this figure pre-immunoprecipitation) and then probing the western transfer membrane with the rat anti-mouse α-tubulin monoclonal antibody. (**E**) Polyclonal anti-pThr555 CRMP-2 antibody reactivity was demonstrated by double immunofluorescence staining on 10 μm cryostat sections showing co-localization with degenerating spinal cord axons from EAE-induced mice immunostained with the monoclonal βIII-tubulin antibody (disassembled, monomeric tubulin; arrows) in axons. DAPI stain shows mononuclear cell infiltrate surrounding lesion (arrowheads). Scale bar = 20 μm. dpi = days post-injection; IP = immunoprecipitation.

(continued)

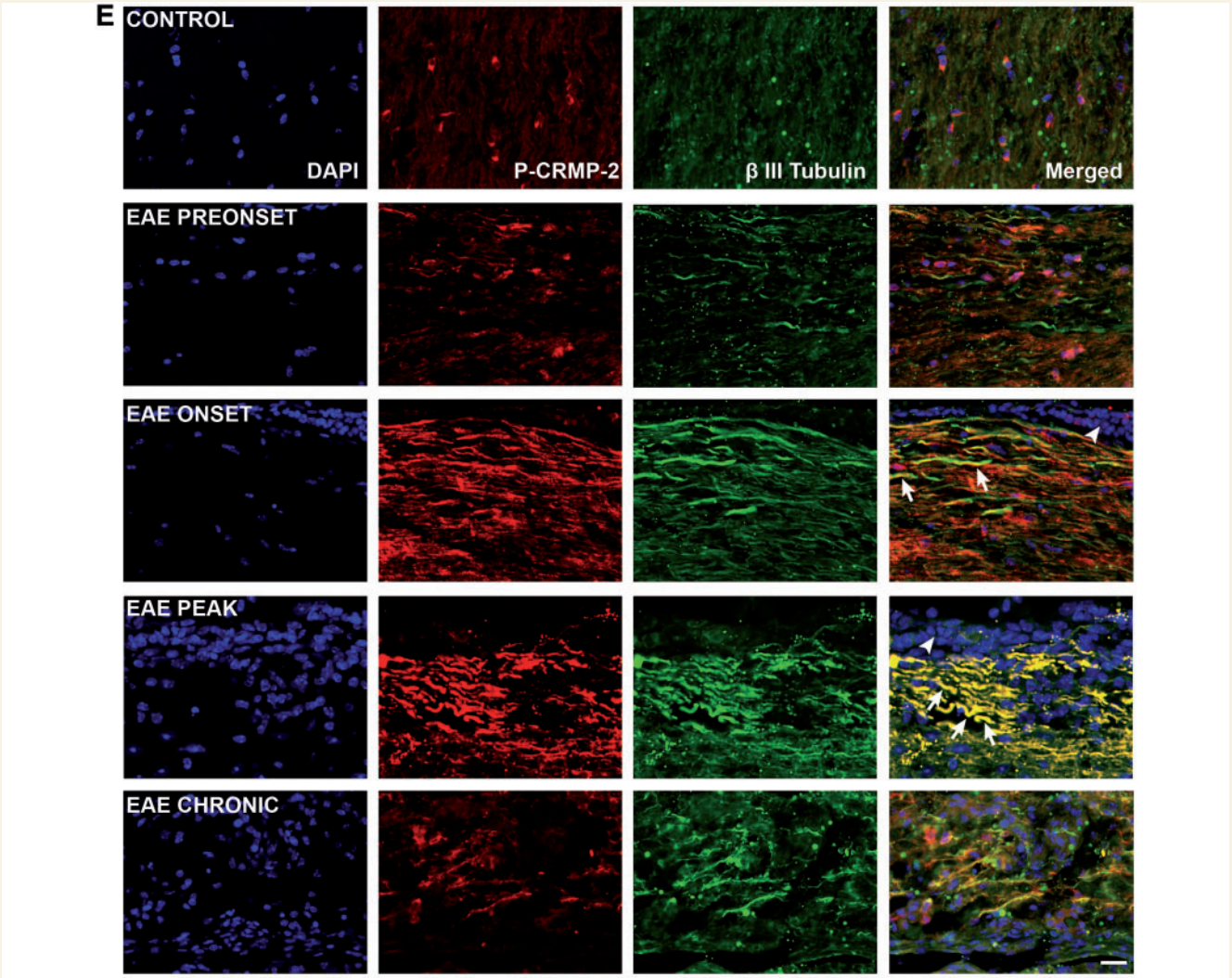

Figure 1 Continued.

sclerosis lesions showed pThr555CRMP-2 staining (Fig. 2G–N). Axonal retraction bulbs could be seen immunostained for pThr555CRMP-2 (Fig. 2L–N). Furthermore, degenerative AT8 hyperphosphorylated tau-positive axons also showed co-localization with pThr555CRMP-2 (Fig. 2Q–Si). No co-staining could be detected for either NF200- and AT8-positive axons and neurons in the spinal cord with pThr514CRMP-2 (GSK3β phosphorylation site; Supplementary Fig. 2C–I). Hence, collectively the data suggest a direct relationship of inflammatory-mediated demyelination and neurodegeneration with pThr555CRMP-2 in neurons and axons.

Deletion of the *ngr1* allele (exon 2) limits the progression of EAE, axonal degeneration and phosphorylation of CRMP-2

We next investigated the possibility that limiting the phosphorylation of CRMP-2 during EAE will limit the progressive neurodegenerative changes that occur in these mice. We first demonstrated that following EAE-induction, the $ngr1^{-/-}$ mice displayed a shift in the time-point of disease onset when compared with the $ngr1^{+/+}$ mice (Fig. 3A and B; Supplementary Table 2A). The $ngr1^{-/-}$ mice showed induction of disease by 15–16 days post-$MOG_{35–55}$ immunization compared with the $ngr1^{+/+}$ mice, which displayed onset of EAE by 12–13 days post-injection (Fig. 3A and Supplementary Table 2). Importantly, the majority of the $ngr1^{+/+}$ mice manifested significant disease (12 of 14 mice) by 18 days post-injection, corresponding to peak neurological deficit with a clinical score of 1.93 ± 0.23 (Fig. 3A and Supplementary Table 2). However, of the $ngr1^{-/-}$ EAE-immunized mice, only 6 of the 16 mice displayed disease symptoms. Moreover, peak severity of the clinical signs occurred at clinical score 1.0 ± 0.34 by 19 days post-injection (Fig. 3A and Supplementary Table 2). This was associated with a reduction in the histopathological parameters for the $ngr1^{-/-}$ mice, which coincided with the progressive neurological decline post-$MOG_{35–55}$-immunization (Fig. 3B and Supplementary Table 2B). Notably, there was a reduction in the score for inflammatory

cell infiltrates, demyelination and axonal degeneration in the EAE-induced *ngr1*$^{-/-}$ mice (Fig. 3B and Supplementary Table 2). These parameters were associated with a reduction in the molecular marker of axonal degeneration, abnormally phosphorylated tau (hyperphosphorylated tau, AT8; Supplementary Fig. 3A). Moreover, following the isolation of the insoluble proteins from spinal cord lysates of EAE-immunized mice (Anderson *et al*., 2008), we found that the $MOG_{35–55}$-induced *ngr1*$^{-/-}$ mice had reduced levels of AT8-positive tau, as compared with the EAE-induced *ngr1*$^{+/+}$ mice (Supplementary Fig. 3A). These findings were associated with an increase in the soluble forms of tau in the *ngr1*$^{+/+}$ compared with the *ngr1*$^{-/-}$ mice,

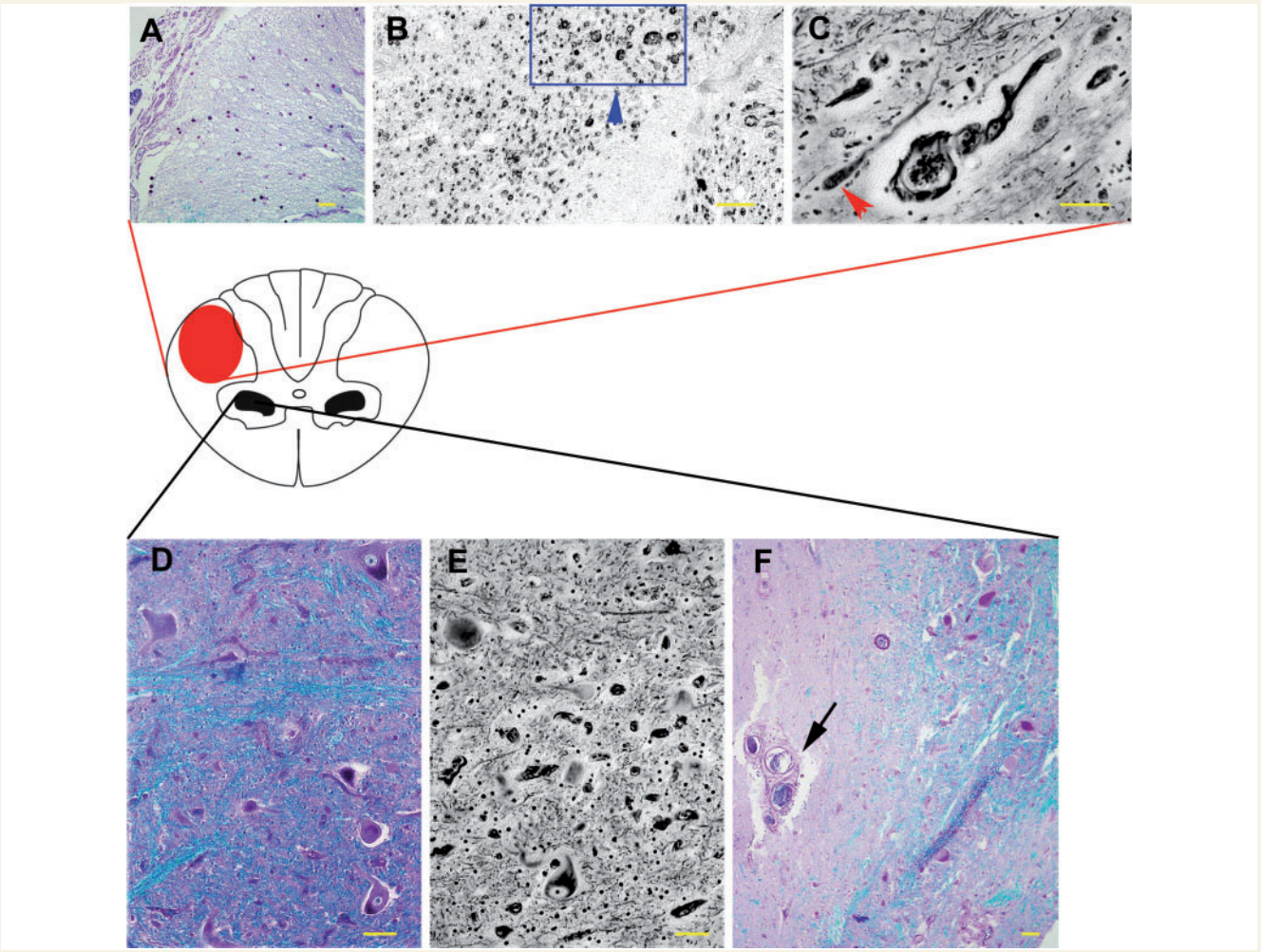

Figure 2 Localization of pThr555CRMP-2 in degenerating neuron somata and axons in chronic-active multiple sclerosis lesions. (**A**) Chronic-active demyelinating multiple sclerosis lesion in the dorsolateral white matter of the lumbar spinal cord stained with Luxol fast blue and Periodic acid Schiff (scale bar = 50 μm). (**B**) Axonal degeneration (blue box and arrowhead) in the dorsolateral white matter of the lumbar spinal cord from the same chronic-active multiple sclerosis case stained with Bielschowsky stain (scale bar = 50 μm). (**C**) Axonal retraction bulb (red arrowhead) present in the dorsal horn of the same chronic-active multiple sclerosis case stained with Bielschowsky (scale bar = 50 μm). (**A–C**) Drawing of a cross-section through the lumbar spinal cord to illustrate the white matter tracts analysed (solid red circle) and the ventral grey matter lesions (solid black circle; **D–F**). (**D**) Ventral horn degenerative neurons of the lumbar spinal cord stained with Luxol fast blue and Periodic acid Schiff, (**E**) Bielschowsky stain and (**F**) Luxol fast blue and Periodic acid Schiff staining, showing perivenular cuffing and infiltrates in the ventral grey matter (arrow). Scale bar = 50 μm. (**G–J**) Chronic-active demyelinating multiple sclerosis lesion of the lumbar spinal cord counterstained with (**G**) DAPI, immunostained for (**H**) NF200 and (**I**) pThr555CRMP-2; and the merged image (**J**) (scale bar = 50 μm). (**K–M**) The same chronic-active demyelinating multiple sclerosis lesion of the lumbar spinal cord with a closer view of the ventral horn grey matter, counterstained with (**K**) DAPI, immunostained for (**L**) NF200, (**M**) pThr555CRMP-2 and (**N**) the merged image (arrow showing axonal retraction bulb). Scale bar = 50 μm. (**O** and **P**) The same chronic-active demyelinating multiple sclerosis lesion of the lumbar spinal cord with (**O**) secondary anti-mouse Alexafluor® 488 antibody control or (**P**) secondary anti-rabbit Alexafluor® 555 antibody control (scale bar = 50 μm). (**Q–Si**) Degenerative axons in the dorsolateral spinal cord in longitudinal (arrow) and cross-section (arrowheads) immunostained for (**Q**) hyperphosphorylated tau AT8, (**R**) pThr555CRMP-2 and (**S**) merged image and (**Si**) magnified image of the retraction bulb (scale bar = 50 μm). (**T–W**) Ventro-lateral region of the same chronic-active demyelinating multiple sclerosis lesion of the lumbar spinal cord with (**T**) DAPI counterstain, (**U**) CD3-positive T cell infiltrates near (**V**) pThr555CRMP-2 positive axons; (**W**) merged image.

(continued)

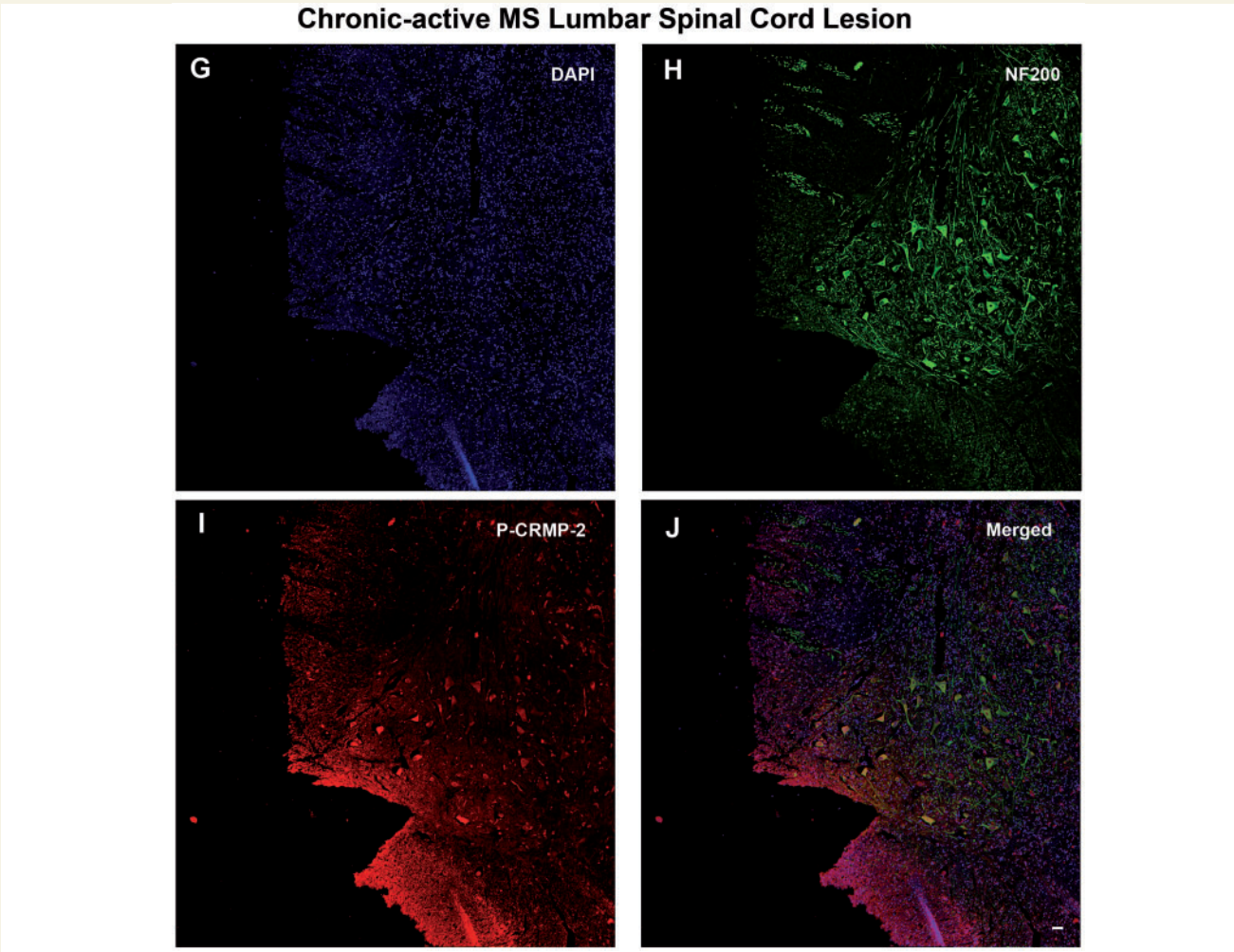

Figure 2 Continued.

(continued)

immunostained with tau-5 (for total tau levels) and normal phosphorylated tau stained with an anti-pSer199/202 tau antibody (Supplementary Fig. 3A). Thus it would appear that in *ngr1*$^{-/-}$ mice, a modest increase in the phosphorylated and hyperphosphorylated forms of tau correlates with axonal degeneration and disease progression.

To further assess the extent of axonal degeneration, we performed ultrastructural analysis on lumbosacral spinal cords of both *ngr1*$^{-/-}$ and *ngr1*$^{+/+}$ mice. As illustrated in Fig. 3C, lesions appearing in the white matter tracts of the spinal cord of *ngr1*$^{+/+}$ mice showed significant axonal degeneration and demyelination with inflammatory infiltrates (Fig. 3C). However, in the spinal cord white matter tracts of *ngr1*$^{-/-}$ mice, there was preservation in axo-myelin integrity along with limited inflammatory infiltrates (Fig. 3C).

The reduced axonal degeneration together with the abrogated neurological decline in the *ngr1*$^{-/-}$ mice following EAE-induction, prompted us to investigate whether spinal cord axons in these mice displayed a reduced propensity to initiate phosphorylation of CRMP-2. Immunofluorescence analysis showed that in the *ngr1*$^{-/-}$ mice there were reduced levels of pThr555CRMP-2 in axons in the longitudinal white matter tracts during EAE (Supplementary Fig. 3B). We showed that neurofilament NF200-positive axons (particularly those showing axonal-spheroids) co-localized significantly with pThr555CRMP-2 immunofluorescence at peak and chronic stages of EAE in *ngr1*$^{+/+}$ mice (Supplementary Fig. 3B). These data suggest that during the progression of EAE there are greater levels of pThr555CRMP-2 in degenerative axons in the spinal cords of *ngr1*$^{+/+}$ compared with *ngr1*$^{-/-}$ mice.

In order to quantitate these changes, we performed co-immunoprecipitation and western blotting from spinal cord lysates of *ngr1*$^{+/+}$ and *ngr1*$^{-/-}$ mice during EAE. We found that the *ngr1*$^{+/+}$ mice had an incremental increase in pThr555CRMP-2 levels, compared with *ngr1*$^{-/-}$ mice during the progression of EAE (Fig. 3D and E). This increase was also evident in the 75 kDa N-terminal variant of the protein, which did not appear in the *ngr1*$^{-/-}$ mice during EAE (Fig. 3D). Importantly, the levels of CRMP-2-associated tubulin were reduced in the *ngr1*$^{+/+}$ but not in the *ngr1*$^{-/-}$ mice during EAE (Fig. 3F and G). The data can be interpreted as increased dissociation of monomeric tubulin from CRMP-2 in the *ngr1*$^{+/+}$ [from $19.75 \pm 2.83\%$ at pre-onset

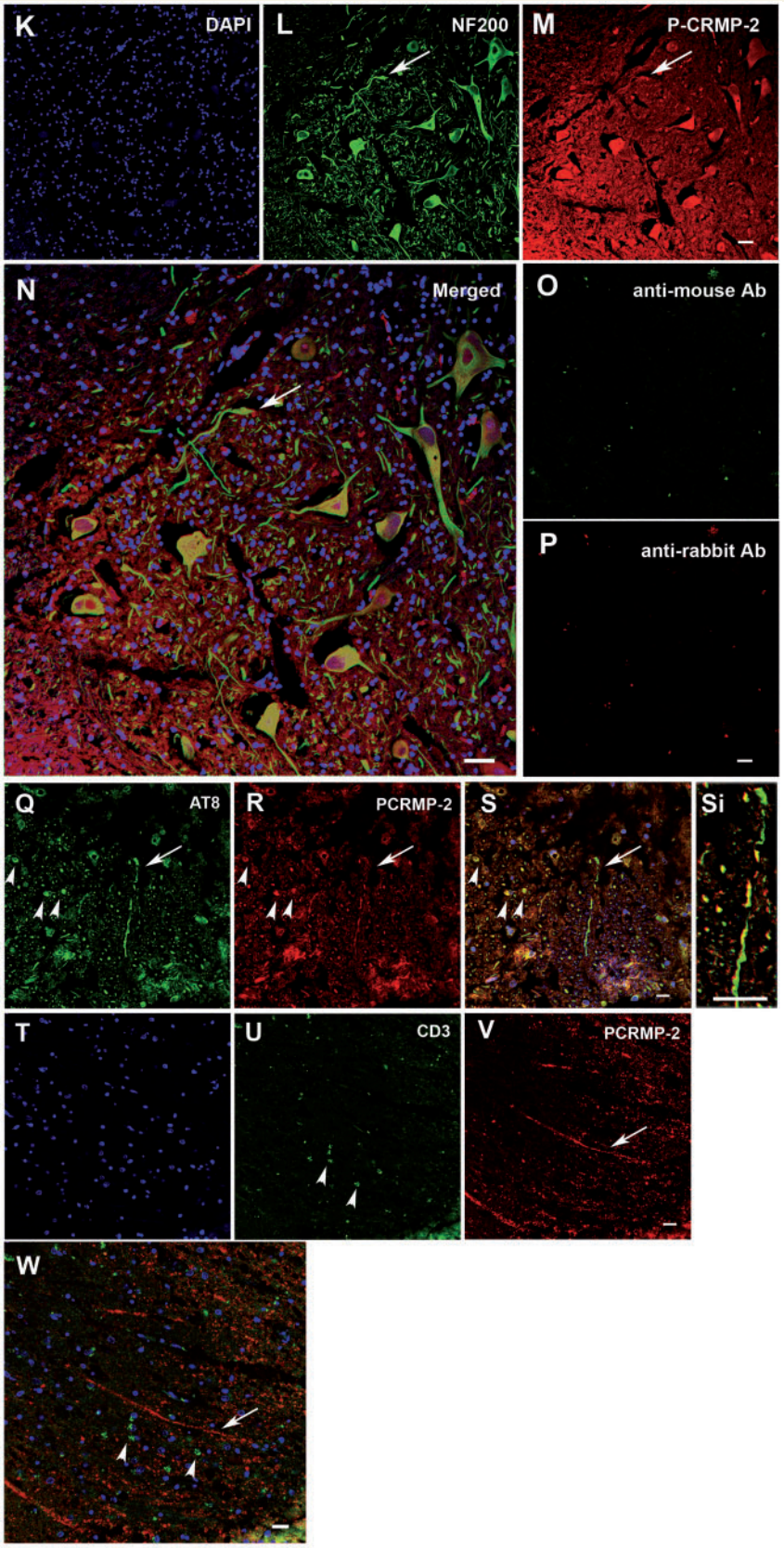

Figure 2 Continued.

Table 2 Human brain tissue collected from individuals with and without other neurological diseases[a]

Patient No.	Sex	Age (years)	Histopathological assessment	Duration of disease	Tissue location	No. of blocks taken at autopsy	*PThr555CRMP2* + immunopositivity
1	F	45	Epileptic; Temporal lobe lesion	N/A	4	1	–
2	F	53	Progressive multifocal leukoencephalopathy	3 weeks	4	1	–
3	F	39	Progressive multifocal leukoencephalopathy	9 years	1	2	–
4	F	41	Progressive multifocal leukoencephalopathy	2 years	1	1	–
5	N/A	N/A	Alzheimer's disease	N/A	1	1	+
6	N/A	N/A	Alzheimer's disease	N/A	1	1	+
7	N/A	N/A	Meningitis	N/A	1	2	+
8	F	83	Non-neurological disease control	N/A	2	2	–
9	M	78	Non-neurological disease control	N/A	2	1	–
10	M	74	Non-neurological disease control	N/A	2	1	–
11	F	82	Non-neurological disease control	N/A	2	1	–
12	N/A	N/A	Non-neurological disease control	N/A	1	1	–
13	N/A	N/A	Non-neurological disease control	N/A	1	1	–
14	N/A	N/A	Non-neurological disease control	N/A	1	1	–
15	N/A	N/A	Non-neurological disease control	N/A	1	1	–
16	N/A	N/A	Non-neurological disease control	N/A	1	1	–
17	N/A	N/A	Non-neurological disease control	N/A	1	1	–
18	N/A	N/A	Non-neurological disease control	N/A	1	1	–

a Post-mortem delay <24 h; biopsy delay <1 h.
N/A = not applicable/not available; 1 = frontal lobe white matter; 2 = periventricular white matter, including subventricular zone of the anterior horn of the lateral ventricle; 3 = internal capsule including striatum; 4 = temporal lobe deep white matter; 5 = occipital lobe deep white matter; 6 = cerebellum; 7 = midbrain; 8 = rostral pons; 9 = caudal pons; 10 = rostral medulla; 11 = caudal medulla; 12 = cervical cord; 13 = thoracic cord; 14 = lumbar cord, as determined by morphological appearance under haematoxylin and eosin staining by neuropathologist.

($P < 0.001$) to $33.77 \pm 3.187\%$ at peak ($P < 0.001$); Fig. 3G] as the levels of CRMP-2 phosphorylation increase during the progression of EAE disease [from $39.16 \pm 49.62\%$ in adjuvant injected *ngr1*$^{+/+}$ mice to $382 \pm 94.41\%$ at peak ($P < 0.05$); Fig. 3E]. However, deletion of the *ngr1* gene limits the EAE-dependent phosphorylation (Fig. 3D and E), replenishing the tubulin association levels (Fig. 3F and G).

Axonal damage and CRMP-2 phosphorylation in the optic nerve of EAE-induced mice

To obtain a direct and quantitative measurement of demyelination and axonal pathology, we stained semi-thin optic nerve cross-sections with toluidine blue and assessed both axon/myelinated fibre diameter and degeneration/loss, between EAE-induced *ngr1*$^{-/-}$ and *ngr1*$^{+/+}$ mice. Toluidine blue staining clearly demonstrated axo-myelin degeneration in a number of axons from pre-onset and onset stages of EAE in the *ngr1*$^{+/+}$ but not in the *ngr1*$^{-/-}$ mice (Fig. 4A and Supplementary Fig. 5). As indicated by the most severe axonal degeneration/loss, the greatest ultrastructural abnormalities were found at peak and chronic stages of EAE, in *ngr1*$^{+/+}$ mice (Fig. 4A). Optic nerve cross-sections were also investigated for lamellated myelin structure, relative to ensheathed large and small calibre axons, by calculating *G*-ratios (Fig. 4B). There was a significant, incremental increase in the optic nerve *G*-ratios of EAE-induced *ngr1*$^{+/+}$ mice with disease progression (from 0.768 ± 0.004 at pre-onset to 0.799 ± 0.004 at peak; Fig. 4B). However, in *ngr1*$^{-/-}$ mice, there was a moderate but comparable increase in the *G*-ratio at pre-onset of disease (from 0.761 ± 0.003 at pre-onset), but neared basal levels by peak (0.705 ± 0.003; Fig. 4B). The overall increase in demyelination was $11.43 \pm 0.597\%$ in adjuvant injected controls (basal level) from the optic nerves of EAE-induced *ngr1*$^{+/+}$ mice by peak of disease, compared with a $-1.651 \pm 0.472\%$ change in demyelination in EAE-induced *ngr1*$^{-/-}$ mice at the same time-point (Fig. 4B). However, there was demonstrable demyelination in the optic nerves of *ngr1*$^{-/-}$ mice at the earliest investigated time-point (Day 7 post-EAE induction), resembling that seen in the *ngr1*$^{+/+}$ mice ($6.123 \pm 0.437\%$ versus $7.096 \pm 0.490\%$, respectively). Interpretation of the data would be that there is an initial thinning of lamellated myelin surrounding axons in the optic nerves in both genotypes that is eventually repaired in the *ngr1*$^{-/-}$ mice by Days 12 to 18 (onset and peak, respectively).

However, we did find an increase in the axonal diameter without compensatory increases in the thickness of myelin that normally occurs during development, with larger calibre axons (ffrench-Constant *et al*., 2004). To exclude the possibility that the optic nerves of *ngr1*$^{-/-}$ mice exhibited thinly myelinated but larger calibre axons, we plotted the axonal diameter measurements during EAE, of the *ngr1*$^{+/+}$ and *ngr1*$^{-/-}$ mice (Fig. 4B). We found that in *ngr1*$^{-/-}$ mice, the axonal calibre was at basal levels at Day 7, post-EAE-induction (Fig. 4B). Thus it would appear that the increase in *G*-ratio in the *ngr1*$^{-/-}$ mice at this early time-point of EAE is related to myelin thinning of axons but is then repaired by 12–18 days post-injection (Fig. 4B). There was an incremental rise in the axonal diameter in the *ngr1*$^{+/+}$ mice as EAE progressed, with a sharp rise by peak of disease (from 25.23 ± 0.21 (Arbitrary Units) at Day 7

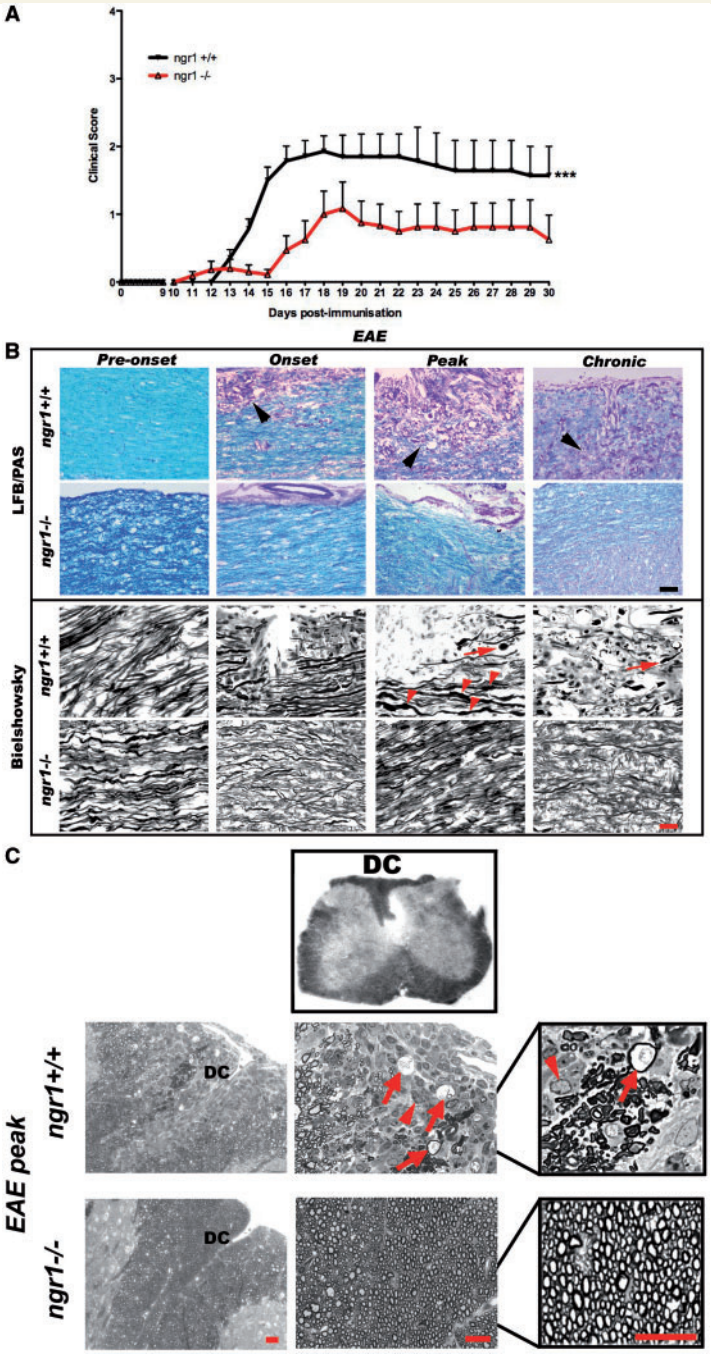

Figure 3 Reduction in EAE disease, axonal degeneration and phosphorylation of CRMP-2 in *ngr1*$^{-/-}$ mice. (**A**) EAE clinical scores after $MOG_{35–55}$-inducion in female C57Bl/6 wild-type littermate (*ngr1*$^{+/+}$, $n = 21$, black line) and *ngr1*$^{-/-}$ mice ($n = 14$ *ngr1*$^{-/-}$, red line; ***$P < 0.001$ repeated measures ANOVA). (**B**) Histopathology of EAE in *ngr1*$^{+/+}$ and *ngr1*$^{-/-}$ mice at pre-onset, onset, peak and chronic stages. Luxol fast blue (LFB) and Periodic acid Schiff (PAS) stain showing inflammatory demyelination and Bielschowsky stain to demonstrate axonal degeneration/loss (arrows show axonal swelling; arrowhead shows an axonal retraction bulb; scale bar = 20 μm). (**C**) Representative semi-thin (1 μm) lumbosacral spinal cord sections from EAE-induced *ngr1*$^{+/+}$ and *ngr1*$^{-/-}$ mice demonstrating significant axonal degeneration in the dorsal column (DC) white matter tracts of *ngr1*$^{+/+}$ mice (arrows) at peak of disease. Inflammatory cells are also present in *ngr1*$^{+/+}$ mice (arrowheads). Scale bar = 50 μm. (**D**) Immunoprecipitation of pThr555CRMP-2 of spinal cord lysates from EAE-induced *ngr1*$^{+/+}$ and *ngr1*$^{-/-}$ mice, followed by reprobing of the membranes with the monoclonal anti-CRMP-2 antibody. There is an increase in pThr555 CRMP-2 of both the CRMP-2A and CRMP-2B variants in EAE-immunized *ngr1*$^{+/+}$ mice from pre-onset to peak of disease. No such changes occurred in the *ngr1*$^{-/-}$ mice at the same time-points after $MOG_{35–55}$ challenge. Control lanes include non-specific rabbit IgG polyclonal antibody and pThr555 CRMP-2 (20 μg) peptide spiked in lysate buffer alone.
A pre-immunoprecipitation 5% input of protein from spinal cord lysates show no discernable difference in total levels of CRMP-2.

(continued)

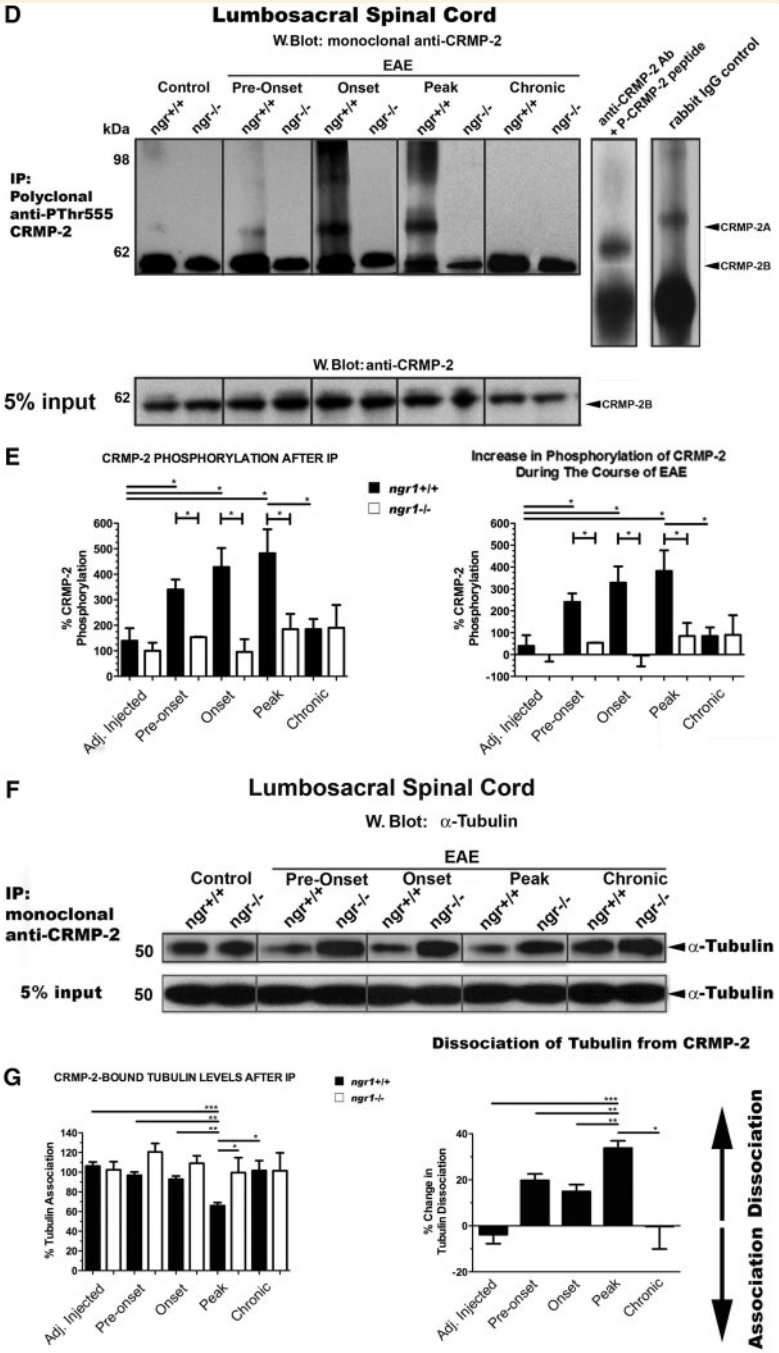

Figure 3 Continued

(**E**) Densitometric quantification of total CRMP-2 and pThr555 CRMP-2B (after immunoprecipitation) from spinal cord lysates of control, *ngr1*$^{+/+}$ and *ngr1*$^{-/-}$ EAE-induced mice, represented as a percentage of basal levels (control uninjected *ngr1*$^{-/-}$ mice; $n = 4$ mice per group and per time-point; $^{*}P < 0.05$ one-way ANOVA). Representation of the percentage change in the levels of pThr555CRMP-2 demonstrates up to a 4-fold increase occurring in *ngr1*$^{+/+}$ EAE-induced mice when compared with *ngr1*$^{-/-}$ mice at peak stage of disease. (**F**) Co-immunoprecipitation of CRMP-2 from spinal cord lysates of control, *ngr1*$^{+/+}$ and *ngr1*$^{-/-}$ EAE-induced mice, showed a decreased association with tubulin in the *ngr1*$^{+/+}$ mice from pre-onset until peak stage of EAE. This finding was not replicated in the *ngr1*$^{-/-}$ EAE-induced mice. (**G**) Densitometric quantification of the levels of CRMP-2-associated tubulin (after immunoprecipitation) from spinal cord lysates of control, *ngr1*$^{+/+}$ and *ngr1*$^{-/-}$ EAE-induced mice, represented as a percentage of basal levels ($n = 4$ mice per group and per time-point; $^{*}P < 0.05$ one-way ANOVA). Representation of the percentage change in the levels of CRMP-2-bound tubulin, demonstrates up to a 3-fold increase in the dissociation of tubulin from CRMP-2 in *ngr1*$^{+/+}$ when compared with *ngr1*$^{-/-}$ EAE-induced mice at peak stage of disease ($^{*}P < 0.05$).

IP = immunoprecipitation.

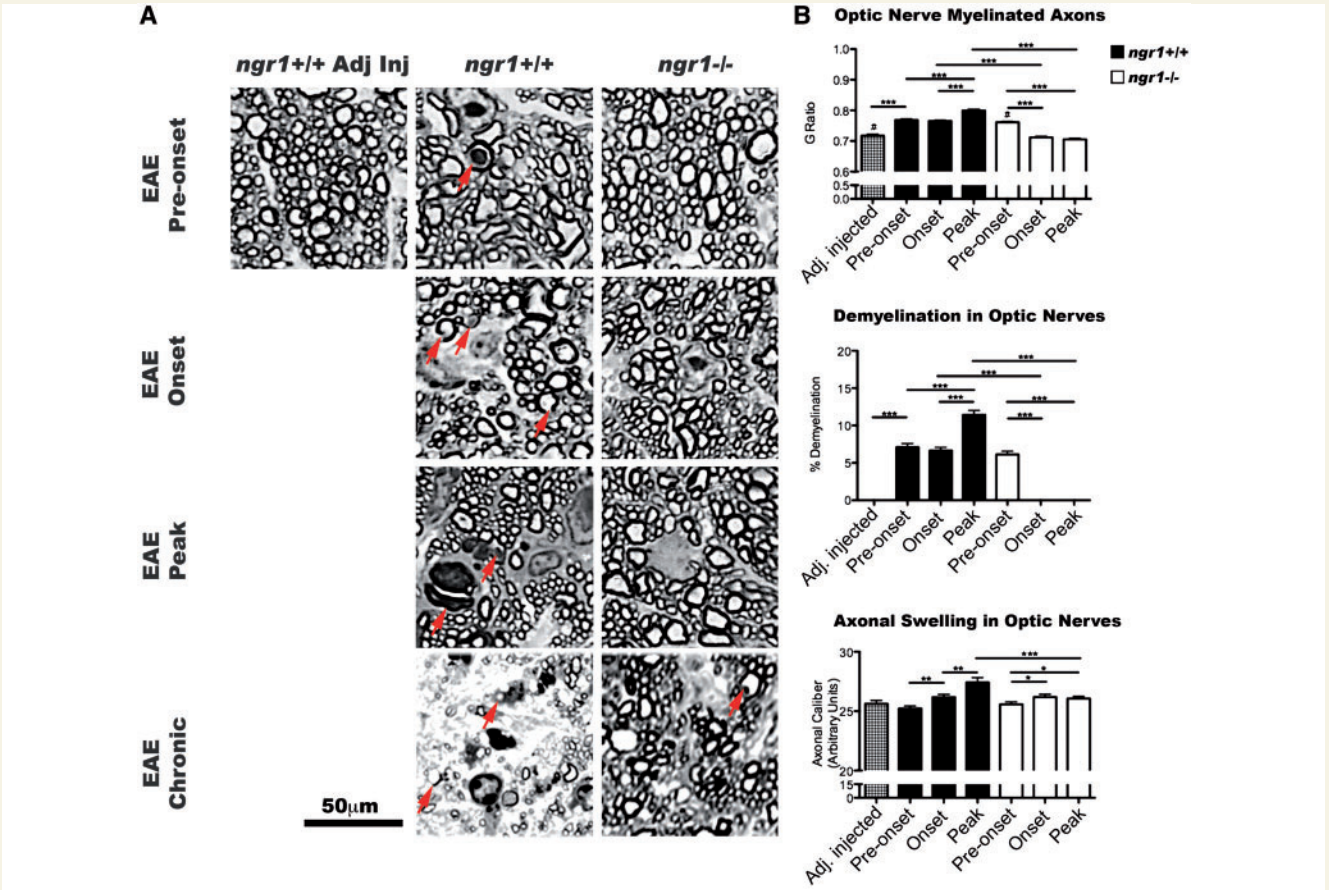

Figure 4 Axonal and myelin damage in EAE-induced *ngr1*$^{-/-}$ mice is reduced and corresponds with abrogated CRMP-2 phosphorylation. (**A**) Semi-thin (1 μm) optic nerve sections of *ngr1*$^{+/+}$ and *ngr1*$^{-/-}$ mice at pre-onset, onset, peak and chronic stages of EAE or adjuvant only injected control mice. Axonal degeneration and demyelination in the *ngr1*$^{+/+}$ EAE-induced mice are present throughout disease, becoming more prevalent at peak (arrows), with significant axonal loss at chronic stage. Perineurial inflammatory infiltrates are a ubiquitous finding in the optic nerves of *ngr1*$^{+/+}$ EAE-mice (arrowhead). These pathological findings are not as evident in the *ngr1*$^{-/-}$ mice. Scale bar = 50 μm. (**B**) Increased demyelination of optic nerves in *ngr1*$^{+/+}$ mice during the course of EAE as determined by *G*-ratios. At pre-onset and onset of EAE, respectively in *ngr1*$^{-/-}$ mice ($n = 3$ mice per genotype, per disease stage and per animal), there is a reduction nearing basal levels (adjuvant injected controls). By peak stage of EAE, there is an increase in the *G*-ratios (i.e. axonal degeneration/demyelination) of *ngr1*$^{+/+}$ mice. The percentage of demyelination is significantly reduced in the *ngr1*$^{-/-}$ after EAE-induction, except at pre-onset stage of disease. Axonal diameters in the optic nerves are increased in *ngr1*$^{+/+}$ mice following EAE-induction. The greatest axonal diameter was demonstrated by peak stage of EAE in *ngr1*$^{+/+}$ mice. In the *ngr1*$^{-/-}$ mice, axonal calibre remains relatively unaltered, with only a modest increase in the axonal diameter by peak stage of disease (***$P < 0.001$, **$P < 0.01$ and *$P < 0.05$ for *ngr1*$^{+/+}$ versus *ngr1*$^{-/-}$ at all time points, analysed by ANOVA with Tukey's *post hoc* test). (**C**) Number of viable myelinated axons in optic nerve semi-thin sections from *ngr1*$^{+/+}$ and *ngr1*$^{-/-}$ mice during the course of EAE ($n = 3$ mice per genotype, per disease stage and per animal). A significant reduction in axonal viability is demonstrated in the *ngr1*$^{+/+}$ by peak stage of EAE (**$P < 0.01$, analysed by one-tailed student's *t*-test). (**D**) Immunoprecipitation of pThr555CRMP-2 of pooled optic nerve lysates from EAE-induced *ngr1*$^{+/+}$ and *ngr1*$^{-/-}$ mice ($n = 6$ per group), followed by reprobing of the membranes with the monoclonal anti-CRMP-2 antibody. There is an increase in pThr555 CRMP-2 of both the CRMP-2A and CRMP-2B variants in EAE-immunized *ngr1*$^{+/+}$ mice at peak of disease. No such changes occurred in the *ngr1*$^{-/-}$ mice at the same time-points after $MOG_{35–55}$ challenge. Control lanes include non-specific rabbit IgG polyclonal antibody and pThr555 CRMP-2 (20 μg) peptide spiked in lysate buffer alone. A pre-immunoprecipitation, 5% input of protein from spinal cord lysates show no discernible difference in total levels of CRMP-2. Densitometric quantification of total CRMP-2 and pThr555 CRMP-2B (after immunoprecipitation) from optic nerve lysates of control, *ngr1*$^{+/+}$ and *ngr1*$^{-/-}$ EAE-induced mice, represented as a percentage of basal levels (control uninjected *ngr1*$^{-/-}$ mice; $n = 6$ mice per group; *$P < 0.05$ one-way ANOVA, **$P < 0.01$). Representation of the percentage change in the levels of pThr555CRMP-2 demonstrates up to a 2-fold increase occurring in *ngr1*$^{+/+}$ EAE-induced mice when compared with *ngr1*$^{-/-}$ mice at peak stage of disease. (**E,** *top*) Co-immunoprecipitation of CRMP-2 from optic nerve lysates of control, *ngr1*$^{+/+}$ and *ngr1*$^{-/-}$ EAE-induced mice, showed a decreased association with tubulin in the *ngr1*$^{+/+}$ mice at peak stage of EAE. This finding was not replicated in the *ngr1*$^{-/-}$ EAE-induced mice. *Left*: Densitometric quantification of the levels of CRMP-2-associated tubulin (after immunoprecipitation) from spinal cord lysates of control, *ngr1*$^{+/+}$ and *ngr1*$^{-/-}$ EAE-induced mice, represented as a percentage of basal levels ($n = 6$ mice per group; *$P < 0.05$ one-way ANOVA). *Right*: Representation of the percentage change in the levels of CRMP-2-bound tubulin, demonstrates an increase in the dissociation of tubulin from CRMP-2 in *ngr1*$^{+/+}$ when compared with *ngr1*$^{-/-}$ EAE-induced mice at peak stage of disease (*$P < 0.05$).

(continued)

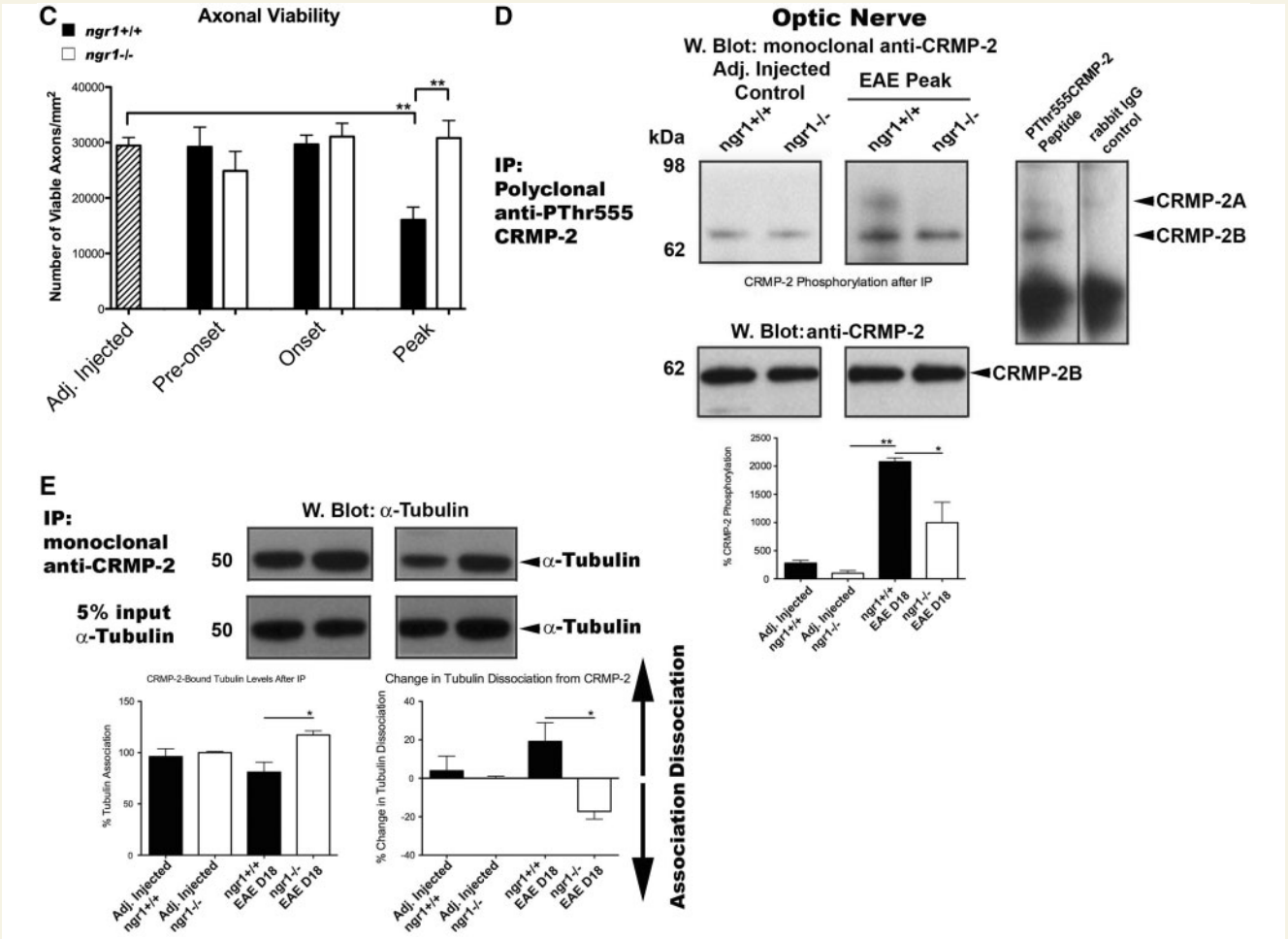

Figure 4 Continued.

to 27.42 ± 0.41 by Day 18 post-EAE induction; Fig. 4B). However, in the optic nerves of *ngr1*$^{-/-}$ mice, there was only a modest increase in axonal diameters by peak stage of EAE, which was just above baseline (26.06 ± 0.19 (Arbitrary Units); Fig. 4B). These data suggest limited axonal swelling in the optic nerves of the *ngr1*$^{-/-}$ mice during EAE.

Highlighting the neurobiological role of the *ngr1* gene, there was an enhanced viability of axons in the optic nerves of *ngr1*$^{-/-}$ mice during EAE (Fig. 4C). We showed that there were no differences in axonal loss in the optic nerves of *ngr1*$^{+/+}$ and *ngr1*$^{-/-}$ mice during the pre-onset and onset stages of EAE (Fig. 4C), although axons had swollen in the *ngr1*$^{+/+}$ EAE-mice (Fig. 4B). However, by peak stage of EAE, we saw a dramatic drop-out of optic nerve axons in the *ngr1*$^{+/+}$ mice (16 048 ± 2316 myelinated axons per square millimetre) that was not replicated in the *ngr1*$^{-/-}$ mice (30 818 ± 3141 myelinated axons per square millimetre, $P < 0.01$; Fig. 4C). Thus we can conclude that there is a preservation of axons in the *ngr1*$^{-/-}$ mice at the peak stage of EAE, correlating with myelin maintenance and a decrease in axonal swelling (Fig. 4B).

We further demonstrated that there was an increase in the phosphorylation of CRMP-2 in the optic nerves of *ngr1*$^{+/+}$ mice by peak stage of EAE (Fig. 4D). These data correlated with significant levels of axo-myelin degeneration and loss in the *ngr1*$^{+/+}$ mice (Fig. 4B and C), showing an ∼2-fold increase of CRMP-2 phosphorylation when compared to the *ngr1*$^{-/-}$ mice at peak stage of EAE (Fig. 4D). The emergence of the 75 kDa pThr555-CRMP-2A band in the *ngr1*$^{+/+}$ optic nerves was again present with EAE-induction but absent in *ngr1*$^{-/-}$ mice (Fig.4D). The levels of tubulin association with CRMP-2 were also reduced in the optic nerves of the *ngr1*$^{+/+}$ mice, correlating with the phosphorylation status of CRMP-2 (Fig. 4D). These data implicate the phosphorylation of CRMP-2 with axonal degeneration during the progression of EAE in the optic nerve of *ngr1*$^{+/+}$ mice and suggest that deletion of the *ngr1* gene limits this molecular mechanism of axo-myelin degeneration from ensuing, in the context of neuroinflammation.

Recombinant AAV2 transduction of retinal ganglion cells with the T555A CRMP-2 mutant construct limits optic nerve axonal degeneration in EAE

Having established that the phosphorylation of CRMP-2 could be reduced in *ngr1*$^{-/-}$ mice at peak stage of EAE, we then addressed

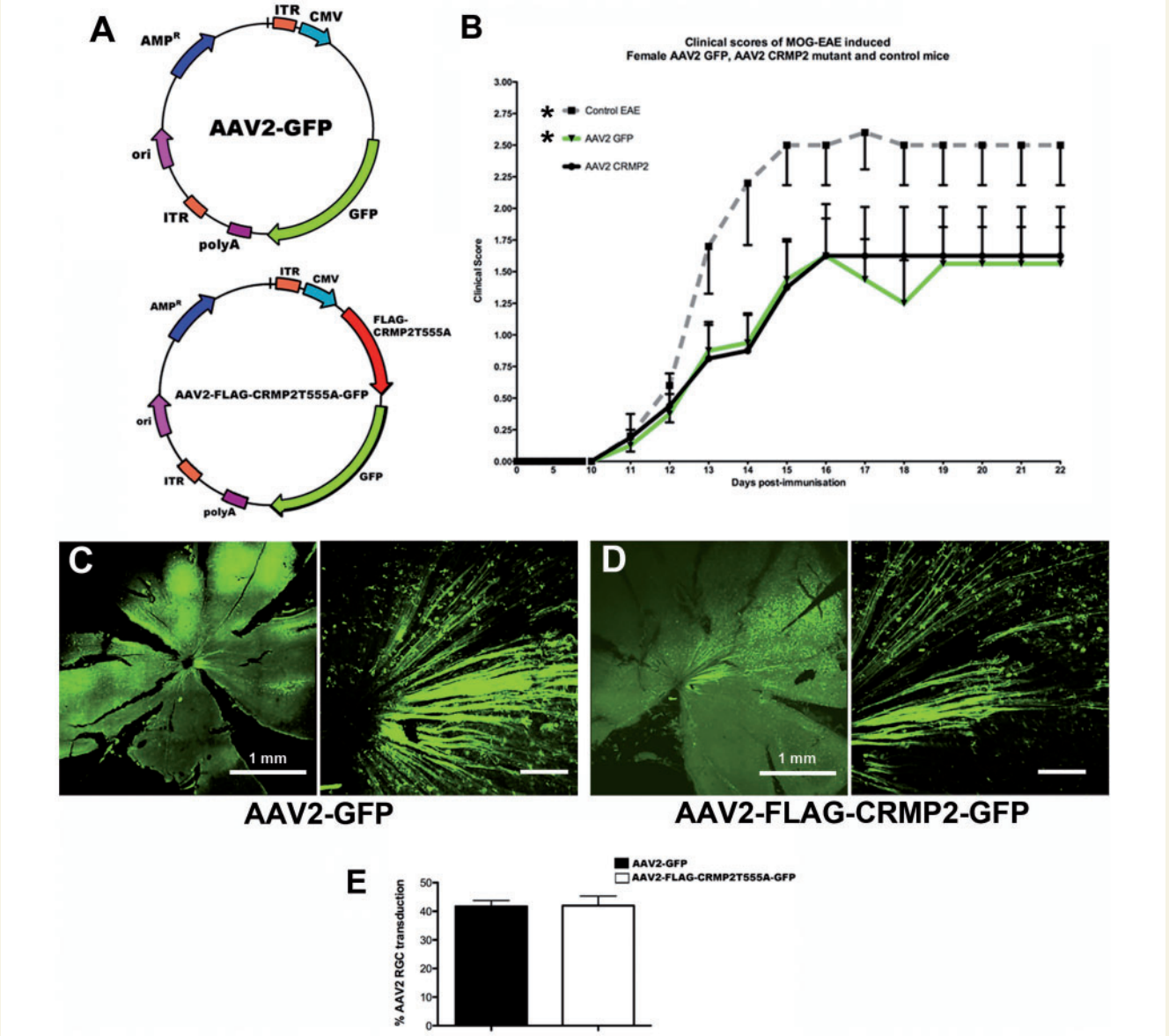

Figure 5 Limiting the phosphorylation of CRMP-2 through a rAAV2 intravitreal delivery system in EAE-induced mice maintains optic nerve axonal integrity. (**A**) Map of the vector construct inserted into a rAAV2 (GFP and Flag-T555ACRMP-2, respectively). (**B**) Seven days following intravitreal injections of rAAV2-GFP or rAAV2-Flag-CRMP2-GFP ($n = 8$ mice per group), or in uninjected control mice ($n = 5$), EAE was induced using the $MOG_{35–55}$ peptide and then followed until all mice reached peak stage of disease ($^*P < 0.05$ analysed by Friedman's non-parametric repeated measures). (**C** and **D**) Representative retinal whole mounts immunolabelled for GFP, in rAAV2-GFP and rAAV2-Flag-CRMP2-GFP injected mice, respectively. (**E**) The percentage of retinal ganglion cells (RGC) transduced with either rAAV2-GFP or rAAV2-Flag-CRMP2-GFP. (**Fi**) rAAV2-GFP transduced optic nerve axons demonstrating localization of GFP particularly in degenerative/transected axons with evident retraction bulbs (arrows). (**Fii**) Immunolabelling of pThr555CRMP-2 of axons (arrows) in the same optic nerve. (**Fiii**) Co-labelling of GFP and pThr555CRMP-2 degenerative axons in the same optic nerve (arrows) near DAPI-positive inflammatory infiltrates (arrowheads). (**Gi**) rAAV2-Flag-CRMP2-GFP transduced optic nerve axons demonstrating localization of Flag in normal appearing axons with (arrow). (**Gii**) Immunolabelling for pThr555CRMP-2 of axons (arrows), in the same optic nerve. (**Giii**) Lack of co-labelling of Flag and pThr555CRMP-2-positive axons in the same optic nerve near DAPI-positive inflammatory infiltrates (arrowheads). (**H**) Estimated numbers of transduced and morphologically degenerative axons per mm^2 of optic nerve tissue in either rAAV2-GFP or rAAV2-Flag-CRMP2-GFP transduced mice (*left*, $^{**}P < 0.002$, analysed by one-tailed student's *t*-test). The percentage of degenerative transduced axons in optic nerves of rAAV2-GFP or rAAV2-Flag-CRMP2-GFP transduced mice demonstrating a 10-fold reduction in the later (*right*, $^{**}P = 0.008$, analysed by one-tailed student's *t*-test). (**I**) Profound axonal retraction bulbs/spheroids in rAAV2-GFP (arrows) compared with more linear intact axons in rAAV2-Flag-CRMP2-GFP transduced nerves. (**J** and **K**) Amyloid precursor protein-positive axons in optic nerves from EAE-induced mice, with and without rAAV2-GFP injection (arrows), co-labelling with pThr555 CRMP-2 (arrows), near DAPI-positive inflammatory infiltrates. (**L**) Reduced amyloid precursor protein-immunopositive axons in rAAV2-Flag-CRMP2-GFP transduced nerves (arrows). Scale bar = 1 mm for low magnification and 50 μm for high magnification.

(continued)

the question whether an abrogation in this phosphorylation may be protective against neuroinflammatory-mediated axonal damage. A rAAV2 expressing both a site-specific mutant form of CRMP-2 (Flag-T555ACRMP2) and GFP or AAV2-GFP control (Fig. 5A) were intraocularly injected into the left temporal eye quadrant of female wild-type C57Bl/6 mice ($n = 8$ per group) and then EAE induced after 1 week to allow for efficient transduction of retinal ganglion cells. The mice developed disease onset and progression to peak stage of disease at least by Day 21, post-EAE induction (Fig. 5B). We achieved an average of ~40% rAAV2-transduction of each retina with either vector (Fig. 5C–E). GFP-labelled optic nerve axons near inflammatory lesions (Fig. 5Fiii and Supplementary Fig. 6B) could be observed to be degenerative in EAE-induced mice, injected intraocularly with rAAV2-GFP (Fig. 5Fi). Many of these degenerative, GFP-expressing axons also demonstrated pThr555-CRMP-2 co-localization (Fig. 5Fii, iii and Supplementary Fig. 6B). In the rAAV2 Flag-T555ACRMP2-GFP transduced retinal ganglion cells, optic nerve axons did not display significant degeneration (Fig. 5G and Supplementary Fig. 6C) or pThr555CRMP-2 co-labelling (Fig. 5G and Supplementary Fig. 6C) even though these axons resided near inflammatory lesions (Fig. 5G and Supplementary Fig. 6C). However, non-transduced axons near inflammatory lesions did display pThr555CRMP-2 localization (Fig. 5G). Analysis of the numbers of transduced axons demonstrating extant axonal degeneration (axonal spheroids/retraction bulbs) (Fig. 5I) showed that there were an estimated 185 ± 24 degenerative axons of the total number of 1106 ± 2258 transduced axons per square millimetre in the rAAV2-GFP optic nerves (Fig. 5H). This compared to an estimated 28 ± 10 degenerative axons of the total number of 1557 ± 383 transduced axons per square millimetre in the rAAV2 Flag-T555ACRMP2-GFP optic nerves (Fig. 5H). These data translate to an average of $20 \pm 3\%$ and $2 \pm 1\%$ of degenerative transduced axons in rAAV2-GFP and rAAV2 Flag-T555ACRMP2-GFP optic nerves, respectively ($P = 0.008$, Fig. 5H). Moreover, co-labelling of these axons with an anti-amyloid precursor protein antibody showed uniform amyloid precursor protein localization of rAAV2 Flag-T555ACRMP2-GFP transduced axons (Fig. 5L), suggesting an intact fast axonal transport mechanism in the transduced axons. However, the fidelity of the fast axonal transport of amyloid precursor protein was clearly compromised in the rAAV2-GFP transduced optic nerve axons, with accumulation of amyloid precursor protein in distended axonal segments (Fig. 5K). Furthermore, the accumulation of amyloid precursor protein could

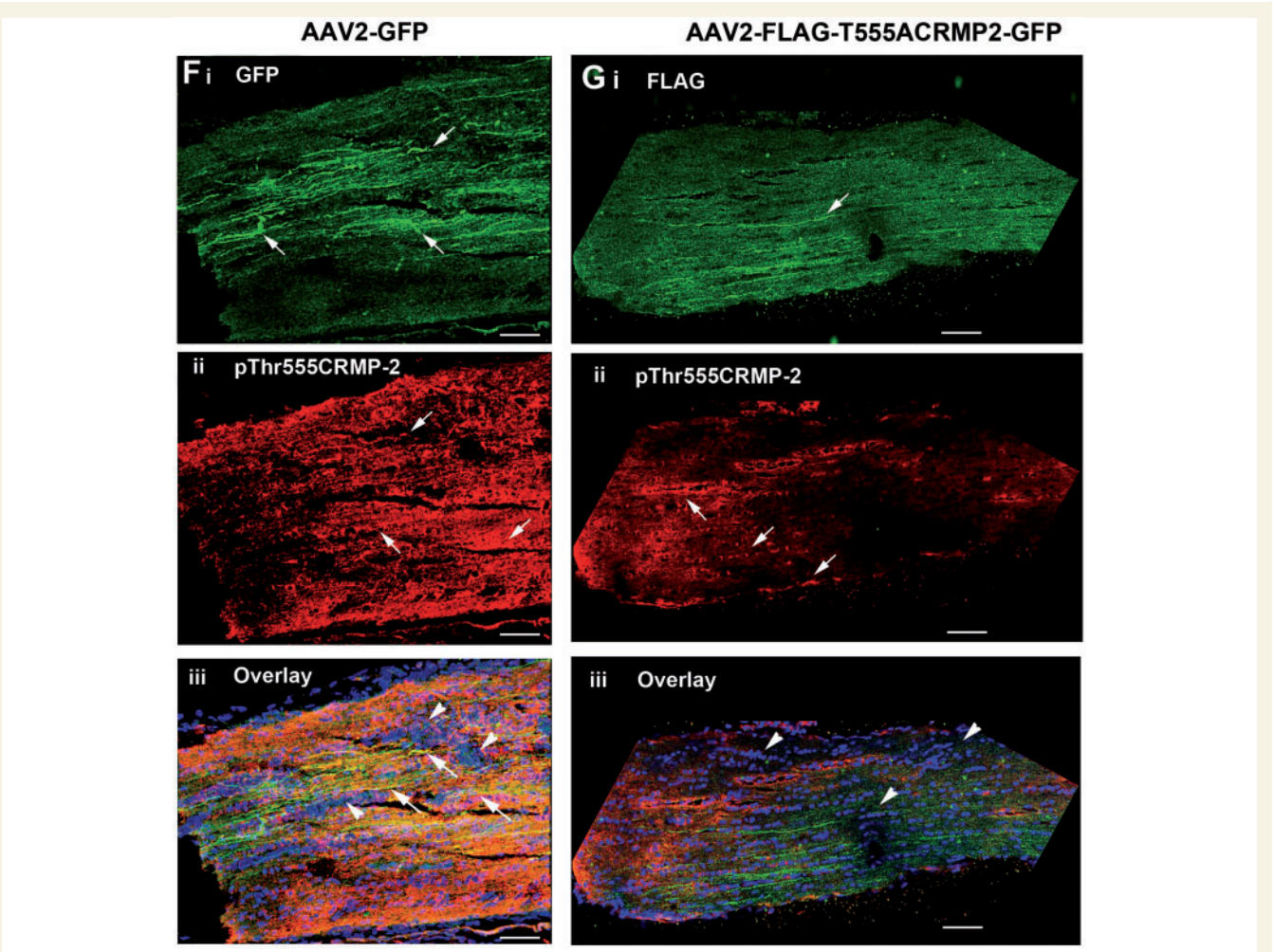

Figure 5 Continued.

(continued)

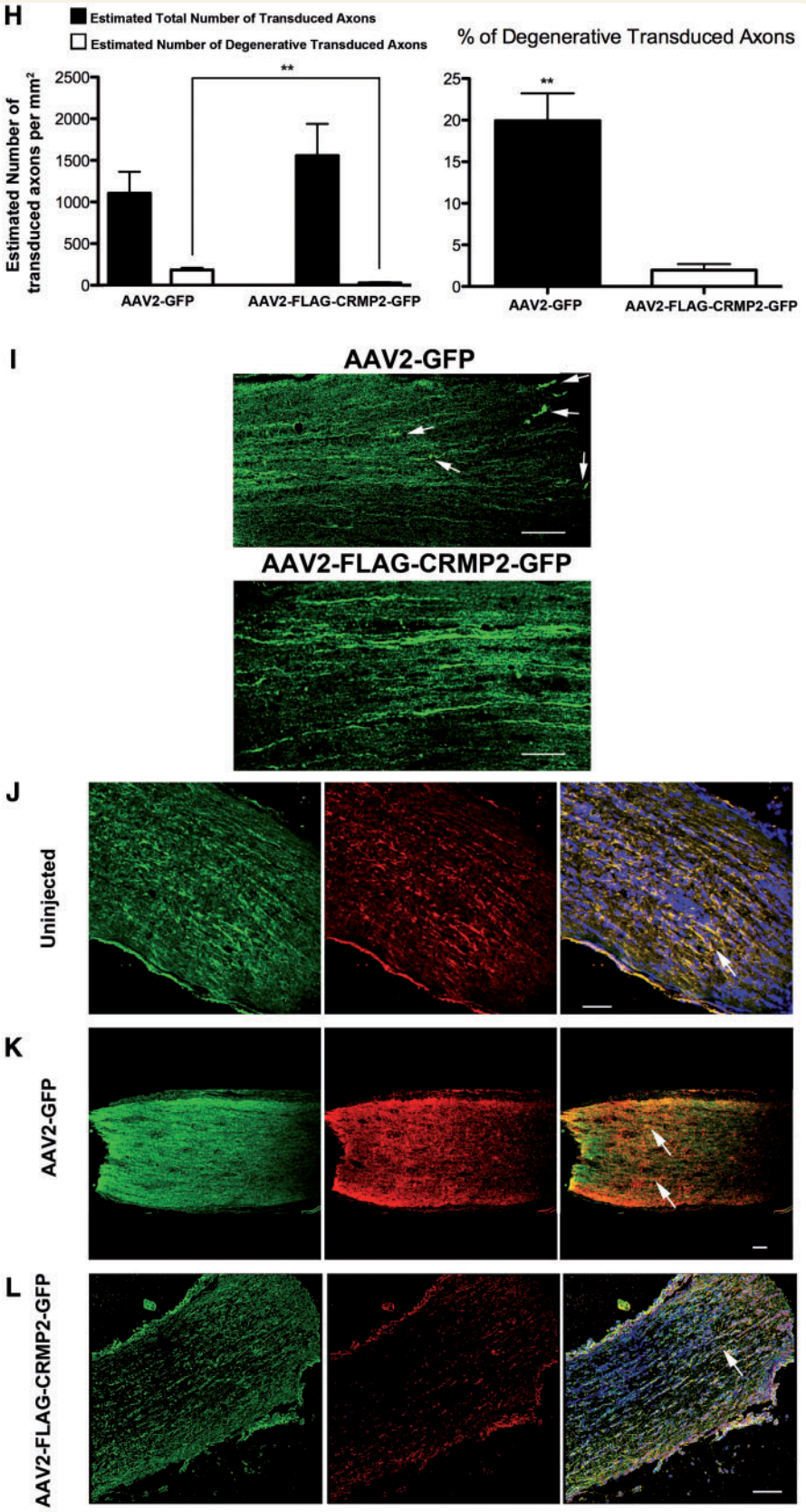

Figure 5 Continued.

also be demonstrated to co-localize with pThr555CRMP-2 in non-transduced optic nerves from EAE-induced mice at peak stage of disease (Fig. 5L, arrow). These data suggest that rAAV2 transduction of retinal ganglion cells with a phospho-mutant form of CRMP-2 (T555ACRMP2), during the peak stage of EAE disease, can limit the axonal degeneration in the optic nerve.

Therapeutic administration of anti-Nogo-A antibodies prevents clinical progression, axonal degeneration and CRMP-2 phosphorylation in EAE

Our previous work has supported the notion that inhibition of Nogo-A in EAE limits axonal degeneration and disease progression (Karnezis *et al*., 2004). Therefore, we next ascertained whether the mechanism governing the limitation of axonal degeneration in Nogo-A passively vaccinated EAE-induced mice (Karnezis *et al*., 2004) was because of a limitation in phosphorylation of CRMP-2. We performed the therapeutic administration of the anti-Nogo(623–640) antibody in female wild-type mice following the induction of $MOG_{35–55}$-EAE (Fig. 6A). A significant delay in the onset of EAE clinical signs could be demonstrated in the anti-Nogo(623–640) antibody treated mice (at 21 days post-induction) when compared with EAE-mice that were treated with a non-specific IgG isotype control or without passive antibody treatment (Fig. 6A). Furthermore, the severity of EAE was also significantly blunted after continuous treatment with anti-Nogo(623–640) antibody (average clinical score of 0.6 ± 0.6 by Day 25 post-induction) compared to the EAE-mice continuously treated with the IgG control antibody (1.8 ± 0.5 by Day 25 post-induction) or without treatment (2.4 ± 0.5 by Day 25 post-induction; Fig. 6A). By the chronic stage of EAE, we also observed a difference in the level of axonal degeneration and demyelination in the spinal cords of the anti-Nogo(623–640) antibody-treated mice compared to the EAE-mice, continuously treated with the IgG control antibody or without treatment (Fig. 6B). Moreover, the abrogation of neurological decline and axonal degeneration demonstrated in the anti-Nogo(623–640) antibody-treated mice correlated with a significant reduction in the level of pThr555CRMP-2 in the spinal cord (Fig. 6C and D). The decrease in the levels of pThr555CRMP-2 correlated with a replenished level of tubulin association with CRMP-2 (Fig. 6C and D). Collectively, these data suggest that the reduction in the neurological decline and associated axonal pathology exhibited by the anti-Nogo(623–640) antibody treatment of EAE-induced mice may be related to a decrease in the phosphorylation status of CRMP-2.

Discussion

Despite the numerous investigative reports of NgR1 signalling in the CNS during disease and injury, there exists debate as to whether the limitation in axonal damage or enhanced regrowth potential is regulated through this mechanism. The current study supports the contention that limiting the NgR1-dependent phosphorylation of CRMP-2 (which normally functions to regulate axonal microtubule assembly), axonal degeneration and hence neurological impairment can be halted in EAE. We have demonstrated that phosphorylated CRMP-2 is localized only in degenerative neuronal somata and axons in chronic-active multiple sclerosis lesions, where myelin damage and inflammatory cells coincide. Our study advocates that targeting NgR1-signalling in EAE, and by extension multiple sclerosis, may be a feasible therapeutic approach to limit the neurodegenerative effects of these conditions.

Current therapeutics in multiple sclerosis target the inflammatory nature of the disease in an attempt to limit the 'autoimmune attack' on CNS myelin and, as a consequence, reduce the devastating neurological complications that characterize this disease. However, comprehensive neuropathological investigations from a vast array of multiple sclerosis brain samples suggest a degree of heterogeneity in the pathogenesis, with some lesions showing tangible neurobiological origins (Lucchinetti *et al*., 2000). Both the 'outside-in' and 'inside-out' hypotheses of demyelination and axonal degeneration involve dysregulation of axo-glial signalling, driving axonal degeneration potentiating neurological decline and establishing disability.

Using the *exon 2 nogo receptor* null mutant mice bred on a C57Bl/6 background (Kim *et al*., 2004), we report that the signalling mechanism that is operative during the neurodegenerative phase of EAE relies on NgR1-dependent phosphorylation of CRMP-2. A significant increase in the phosphorylation of CRMP-2 at the Thr555 site, specific for Rho-associated, coiled-coil containing protein kinase 2 (ROCK2) (Arimura *et al*., 2000; Arimura and Kaibuchi, 2005; Mimura *et al*., 2006), was demonstrated to be operative in EAE. This mechanism has been previously identified to be important in neurite/axon retraction events in culture (Arimura *et al*., 2000; Arimura and Kaibuchi, 2005). Similarly, pThr555-CRMP-2 has been demonstrated to be responsible for axonal degeneration in an acute model of spinal cord injury (Mimura *et al*., 2006). Our finding that levels of pThr555-CRMP-2 in the spinal cord and optic nerve of $ngr1^{+/+}$ but not $ngr1^{-/-}$ mice, incrementally increased during the clinical and pathological progression of EAE, is critical in defining a neurobiological basis for this signalling cascade during neuroinflammatory-mediated degeneration.

There is strong evidence that phosphorylation of CRMP-2, either by GSK-3β, Cdk-5 or ROCK2, inactivates the normal physiological functions of CRMP-2. Physiologically, CRMP-2 can associate with α- and β-tubulin heterodimers (Arimura and Kaibuchi, 2005; Arimura *et al*., 2005), kinesin-1 motor proteins (Kimura *et al*., 2005), TrkB and the Sra/WAVE1 complex, to facilitate anterograde axonal transport, and thereby growth, repair, maintenance and communication (Kawano *et al*., 2005; Arimura *et al*., 2009). Disruption of transport of this molecular cargo is integral for the interruption in the maintenance of the axonal terminal and by extension, synaptic connectivity (Arimura *et al*., 2005, 2009; Kawano *et al*., 2005; Kimura *et al*., 2005; Petratos *et al*., 2010). The consequential loss of axo-dendritic connectivity, mediated through various negative signal transduction events, leads to actin and tubulin depolymerization and eventual axonal retraction (Schmidt and Rathjen, 2010). However, the question

remains as to whether these events can be initiated during neuroinflammatory diseases such as EAE and multiple sclerosis.

Our data suggest that pThr555CRMP-2 is involved as a neurodegenerative molecule of axons and neurons in active multiple sclerosis lesions and that this signal can be limited by ablation of the *NgR1* gene or by therapeutically targeting Nogo-A, during acute neuroinflammation, without any immune-dependent mechanisms being directly responsible for this signalling. However, we did observe that the phosphorylation of CRMP-2 was reduced at the chronic stage of EAE, a stage where neurodegeneration continues to progress. We are currently investigating this finding to delineate whether there is a clearance of extracellular myelin-associated inhibitory factors or NgR1 expression changes at the chronic stage of EAE. However, one line of

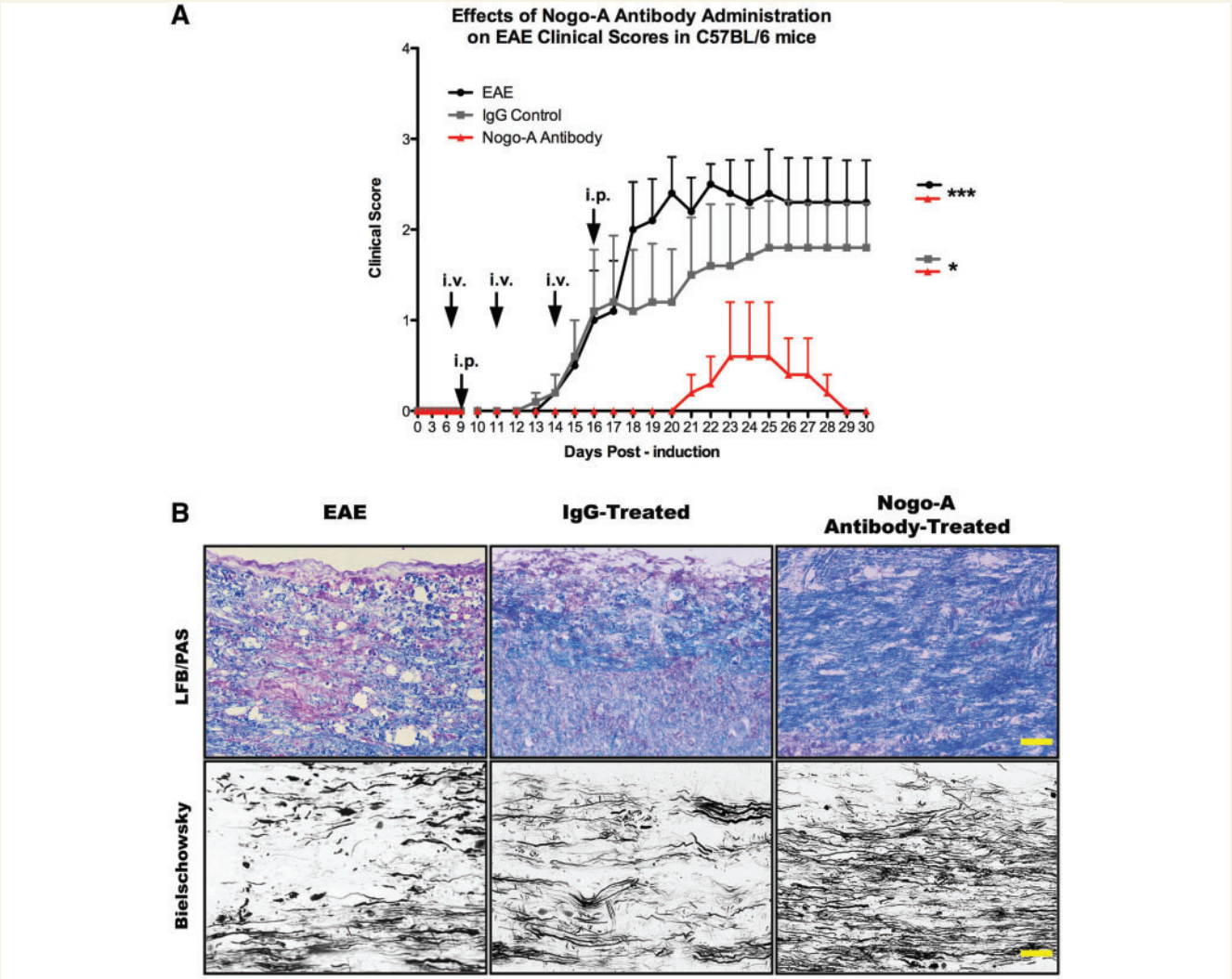

Figure 6 Therapeutic administration of anti-Nogo-A antibodies prevents clinical progression, axonal degeneration and CRMP-2 phosphorylation in EAE. (**A**) Combination of intravenous (Days 8, 11 and 14) and intraperitoneal (Days 9 and 16) administration of anti-Nogo(623-640) antibody (1 mg per injection), non-specific IgG control antibody or no injection in EAE-induced mice ($n = 8$ mice per group, $***P < 0.001$, $*P < 0.05$ analysed by Friedman's non-parametric repeated measures). (**B**) Histopathological analysis of inflammatory demyelination [Luxol fast blue and Periodic acid Schiff (LFB/PAS) stain] and axonal degeneration (Bielschowsky silver stain) at chronic stage of EAE after either, no treatment regime, IgG or anti-Nogo(623–640) antibody treatment. Staining with Luxol fast blue and Periodic acid Schiff highlights significant sparing of myelin in the Nogo(623–640) antibody treated spinal cord white matter tracts compared to the demyelination in EAE-induced mice with non-specific IgG or without treatment. Importantly, axonal degeneration is also substantially reduced in the Nogo(623–640) antibody treated group. Scale bar = 20 μm. (**C**) Immunoprecipitation of pThr555CRMP-2, demonstrating increased levels in spinal cord lysates from EAE-mice without treatment or treated with IgG antibody. However, substantial reduction is evident following Nogo(623–640) antibody treatment. Co-immunoprecipitation of CRMP-2 shows reduced association of tubulin to CRMP-2 in EAE-induced mice treated with non-specific IgG or without treatment, but CRMP-2-bound tubulin levels are higher in the Nogo(623–640) antibody treatment group. (**D**) Optical density measurements of protein levels show a significant reduction in pThr555CRMP-2 ($*P < 0.05$) that correlate with an increase in tubulin association to CRMP-2 in the Nogo(623–640) antibody treatment group ($n = 8$ mice per group).

(continued)

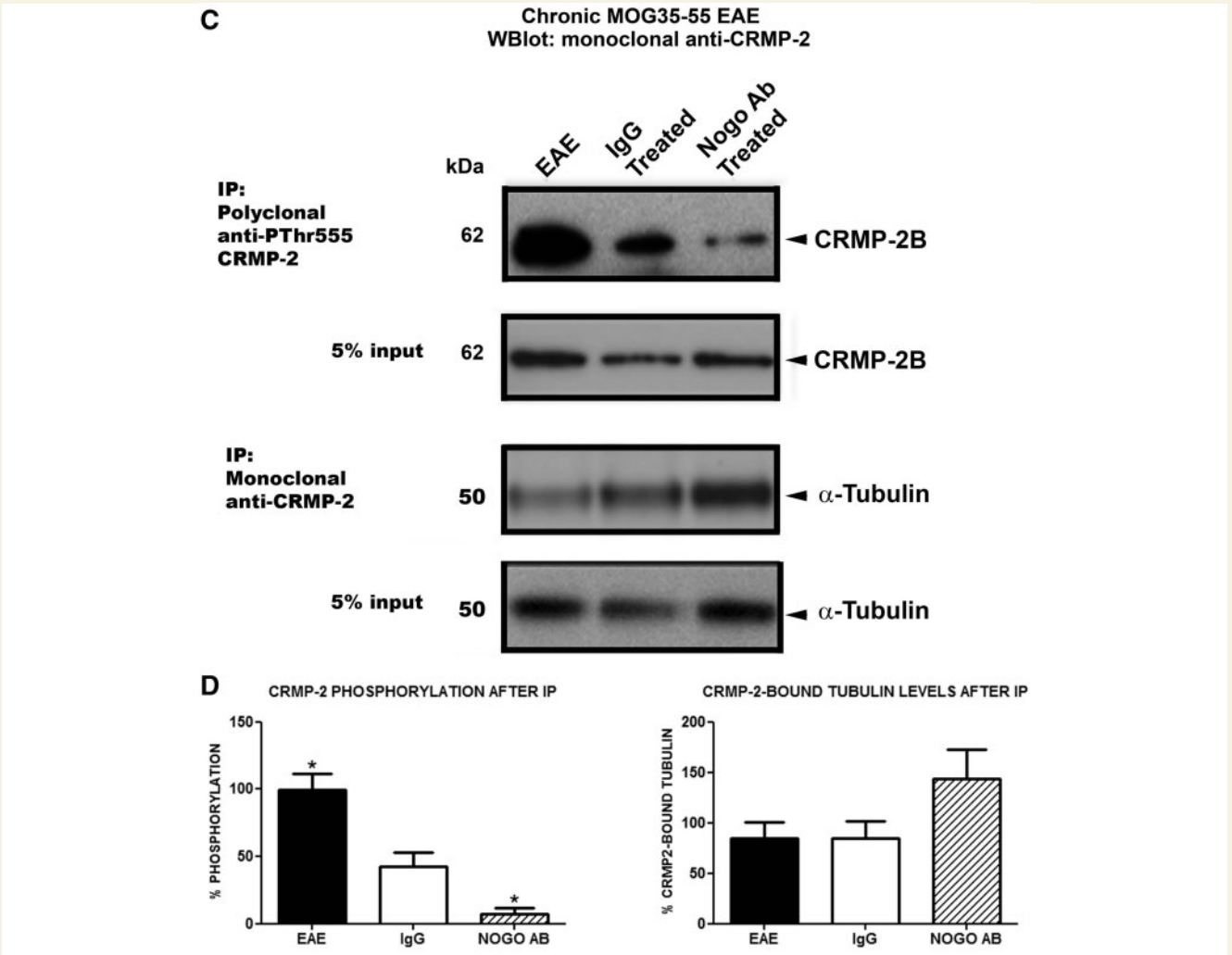

Figure 6 Continued.

investigation may derive from data that show that CRMP-2 is cleaved by calpain during overt neurodegeneration, forming a 55 kDa truncated form (Taghian *et al*., 2012). Such forms of CRMP-2 have been linked to neuronal cell death in various models of neurodegeneration (Taghian *et al*., 2012). Despite the uncertain mechanism occurring during the chronic stage of EAE, we importantly showed that the downstream target of NgR1 signalling, the phosphorylation of CRMP-2 at the Thr555 site, can be abrogated in retinal ganglion cell axons by transduction using a rAAV2 Flag-T555ACRMP2-GFP. The limitation of this signalling cascade during EAE-induced optic neuritis maintains the fidelity of these optic nerve axons and their fast axonal transport mechanisms.

The CNS tissue milieu during injury or disease is rich in axonal outgrowth inhibitors such as Nogo-A, potentiating axonal retraction events and blocking regeneration (Profyris *et al*., 2004). It has recently been shown that limiting NgR1 signalling in the $MOG_{35–55}$-induced or the B10.PL models of EAE, by using small interfering RNA knock-down of *Nogo-A*, can ameliorate the disease severity and enhance axonal repair (through increase in GAP-43-positive axons within the spinal cord) without altering myelin-specific T cell proliferation and cytokine production (Yang *et al*., 2010). Our study extends these findings by pinpointing the signalling mechanism responsible for axonal degeneration in EAE and has demonstrated that downstream pThr555CRMP-2 is present in degenerative neurons and axons of chronic-active multiple sclerosis lesions.

It was recently discovered that the co-receptor of NgR1, Lingo-1, can promote demyelination in the $MOG_{35–55}$ EAE murine model (Mi *et al*., 2007). These investigators showed that in $MOG_{35–55}$-induced *lingo-1*$^{-/-}$ mice or wild-type EAE-induced mice treated with a function-blocking anti-Lingo-1 antibody, demyelination was limited thereby blunting the neurological decline. Although these findings implicate the NgR1 signalling complex in the promotion of demyelination during neuroinflammation, our data suggest that targeting the NgR1 high-affinity receptor for myelin associated inhibitory factor-binding limits axonal degeneration during the onset and peak stages of EAE. However, at the early pre-onset stage of EAE, an equivalent proportion of demyelination in the optic nerves of both the *ngr1*$^{-/-}$ wild-type

littermate mice was demonstrated. This initial thinning of myelin (increasing *G*-ratio) does not persist with progression of disease in the *ngr1*$^{-/-}$ mice, suggesting that possible remyelination may in fact be preserving axons at the early stage of neuroinflammation (Harrington *et al*., 2010). Despite these data, we believe that by limiting the axonal phosphorylation of CRMP-2 during neuroinflammation, we can preserve the axons during the peak stage of EAE as we demonstrated in the optic nerve following the rAAV2 Flag-T555ACRMP2-GFP transduction of retinal ganglion cells. These *in vivo* data for the first time demonstrate that inhibition of the phosphorylation of CRMP-2 can prevent neuroinflammatory-mediated axonal degeneration. We not only demonstrated the limitation of axonal degeneration through the introduction of a site-specific phosphorylation mutant of CRMP-2 but also showed that when the capacity of Nogo-A to bind to its cognate receptor(s) is blocked, the inhibition of axonal degeneration in EAE could limit the phosphorylation of CRMP-2. This suggests that abrogating Nogo-A/NgR1 binding prevents axonal degeneration by blocking CRMP-2 phosphorylation.

Given the recent implication that NgR1 is involved in the efflux of activated macrophages from injured peripheral nerves (Fry *et al*., 2007), we wanted to investigate the possibility of a putative immune role for NgR1 during CNS inflammation. We found no discernible difference in the proliferation response of T cells isolated from *ngr1*$^{-/-}$ and *ngr1*$^{+/+}$ mice at pre-onset, peak and chronic stages of EAE (7, 18 and 30 days post-injection) in response to the $MOG_{35–55}$ peptide (Supplementary Fig. 4). Furthermore, we were unable to demonstrate differences in cytokine profiles from EAE-induced *ngr1*$^{-/-}$ (12 and 18 days post-injection) compared with *ngr1*$^{+/+}$ mice. However, when we analysed the populations of CD3+/CD8+, CD3+/CD4+ and B220 lymphocytes, Gr-1+, F4-80+ and CD-11c+ granulocytes in the spleen and CNS of *ngr1*$^{-/-}$, we could not demonstrate differences in these populations of immune-lineage cells from *ngr1*$^{+/+}$ mice 18 days post-EAE immunization (data not shown). The inference would therefore be that the potential for immune-mediated induction of disease is not altered in the *ngr1*$^{-/-}$ mice. Thus, it would appear that the limitation of the neurological decline in the *ngr1*$^{-/-}$ mice is dependent on a neurobiological mechanism. Despite this, recent data show that monocytes, T and B cells isolated from patients with multiple sclerosis express NgR1 (Pool *et al*., 2009). Given that stimulation of immune cells with Nogo led to an alteration of their adhesion properties, it is possible that in immune cells, NgR1 signalling regulates their cytoskeletal dynamics through RhoA activation (Pool *et al*., 2009). Therefore, further investigation is required to implicate or exclude a role of NgR1 in immune cell activation and migration in multiple sclerosis.

Current evidence defines pharmacological blockade of myelin associated inhibitory factors as a means of enhancing regeneration in the CNS (McGee and Strittmatter, 2003; Zorner and Schwab, 2010). Blocking the signalling of Nogo-A in CNS disease and injury has been well studied and includes EAE (Karnezis *et al*., 2004; Mi *et al*., 2007). In this study, we used the anti-Nogo(623–640) antibody, previously demonstrated to promote axon outgrowth in the presence of the Nogo peptide, as well as the prevention of neurological decline when injected intravenously over the course of EAE (Karnezis *et al*., 2004). We showed that after four injections of anti-Nogo(623–640) antibodies, the decreased severity of EAE correlated with a decreased amount of axonal degeneration. Importantly, reduced levels of pThr555-CRMP-2 in these animals corresponded with replenished tubulin association.

Function-blocking antibodies of Nogo-A have been successfully used in preclinical experiments enhancing locomotor performance in neurotrauma paradigms in rodents and adult monkeys (Schnell and Schwab, 1990; Freund *et al*., 2006), improving manual dexterity after a cervical spinal cord injury in the latter (Freund *et al*., 2006). Over the space of two decades, these significant studies advocating therapeutic targeting of Nogo-A in neurotrauma have encouraged the Phase I clinical trials of anti-human Nogo-A antibody (ATI 355) by Novartis (Kwon *et al*., 2010). With 45 patients enrolled in this study, intrathecal administration of the antibody in these patients has shown remarkable tolerance with no side-effects manifest in this group (Kwon *et al*., 2010). With a Phase II trial currently underway, we now propose that one of the major mechanisms by which anti-Nogo-A antibody treatment is clinically effective may well be through the eventual decrease of the phosphorylated levels of CRMP-2 limiting NgR1-dependent axonal degeneration. Interestingly, other pharmacological studies using the ectodomain of NgR1 and co-receptors such as Lingo-1 have recently shown enhanced neurological improvement in injury and disease models of the CNS by blocking the binding of the myelin associated inhibitory factors (Lee *et al*., 2004; Li *et al*., 2004; Wang *et al*., 2006). It is tantalizing to suggest that similar therapeutic effects could be met in the treatment of multiple sclerosis.

This study has provided new insights into the molecular mechanisms that govern axonal degeneration during inflammatory demyelination of the CNS (as occurs in multiple sclerosis) as well as offering novel therapeutic strategies for this disease. Since myelin damage is a dominant event in neurodegeneration, the work presented here may provide novel therapeutic avenues to attenuate axonal abnormalities, which accompany demyelination in a variety of disorders such as spinal cord and brain injury, stroke and multiple sclerosis. We suggest that blockade of NgR1 signalling and reduction of CRMP-2 phosphorylation limits axonal degeneration in EAE, allowing for the normal physiological function of CRMP-2 to ensue, and by virtue, limiting the axonal degeneration and alleviating clinical symptoms of EAE.

Acknowledgements

Authors would like to acknowledge the assistance of Monash MicroImaging (MMI) for the provision of microscopy instrumentation, training and in particular Stephen Firth, Dr. Judy Callaghan and Dr. Alex Fulcher for their scientific and technical assistance. Authors thank the assistance of Associate Professor Michael F Gonzales, Consultant Neuropathologist, The Royal Melbourne Hospital, Australia, for his assistance in defining the neuropathological cases presented in this manuscript. They would also like to thank Professor Christina Mitchell and Dr. Lisa Ooms (Monash University), as well as Dr. Adam Cole (Garvan Institute of Medical Research) for providing the pRK-5 plasmid CRMP-2

vector. Finally, the authors acknowledge Professor Paul McMenamin for his help in training staff and students in the retinal dissections.

Funding

National Health and Medical Research Council (NHMRC) of Australia [384157, to S.P., 380832 and 436634 to C.C.A.B.]; National Multiple Sclerosis Society of New York [RG 4398A1/1 to S.P. and R.G., 3844A2/1 to C.C.A.B.]; The Baker Foundation [C.C.A.B.]; NHMRC Allied Health Postdoctoral Training Fellowship [M.F.A.]; Multiple Sclerosis Research Australia Vacation Scholarship [K.T.], McDonald Fellowship multiple sclerosis International Federation [S.L.]; Krembil Chair in Neural Repair and Regeneration [M.G.F.].

Supplementary material

Supplementary material is available at *Brain* online.

References

Anderson JM, Hampton DW, Patani R, Pryce G, Crowther RA, Reynolds R, et al. Abnormally phosphorylated tau is associated with neuronal and axonal loss in experimental autoimmune encephalomyelitis and multiple sclerosis. Brain 2008; 131: 1736–48.

Arimura N, Kaibuchi K. Key regulators in neuronal polarity. Neuron 2005; 48: 881–4.

Arimura N, Inagaki N, Chihara K, Menager C, Nakamura N, Amano M, et al. Phosphorylation of collapsin response mediator protein-2 by Rho-kinase. Evidence for two separate signaling pathways for growth cone collapse. J Biol Chem 2000; 275: 23973–80.

Arimura N, Hattori A, Kimura T, Nakamuta S, Funahashi Y, Hirotsune S, et al. CRMP-2 directly binds to cytoplasmic dynein and interferes with its activity. J Neurochem 2009; 111: 380–90.

Arimura N, Menager C, Kawano Y, Yoshimura T, Kawabata S, Hattori A, et al. Phosphorylation by Rho kinase regulates CRMP-2 activity in growth cones. Mol Cell Biol 2005; 25: 9973–84.

Azari MF, Profyris C, Karnezis T, Bernard CC, Small DH, Cheema SS, et al. Leukemia inhibitory factor arrests oligodendrocyte death and demyelination in spinal cord injury. J Neuropathol Exp Neurol 2006; 65: 914–29.

Bernard CC, Johns TG, Slavin A, Ichikawa M, Ewing C, Liu J, et al. Myelin oligodendrocyte glycoprotein: a novel candidate autoantigen in multiple sclerosis. J Mol Med 1997; 75: 77–88.

Cole AR, Noble W, Aalten L, Plattner F, Meimaridou R, Hogan D, et al. Collapsin response mediator protein-2 hyperphosphorylation is an early event in Alzheimer's disease progression. J Neurochem 2007; 103: 1132–144.

ffrench-Constant C, Colognato H, Franklin RJ. Neuroscience. The mysteries of myelin unwrapped. Science 2004; 304: 688–9.

Fournier AE, GrandPre T, Strittmatter SM. Identification of a receptor mediating Nogo-66 inhibition of axonal regeneration. Nature 2001; 409: 341–6.

Freund P, Schmidlin E, Wannier T, Bloch J, Mir A, Schwab ME, et al. Nogo-A-specific antibody treatment enhances sprouting and functional recovery after cervical lesion in adult primates. Nat Med 2006; 12: 790–2.

Fry EJ, Ho C, David S. A role for Nogo receptor in macrophage clearance from injured peripheral nerve. Neuron 2007; 53: 649–62.

GrandPre T, Nakamura F, Vartanian T, Strittmatter SM. Identification of the Nogo inhibitor of axon regeneration as a Reticulon protein. Nature 2000; 403: 439–44.

Gu Y, Hamajima N, Ihara Y. Neurofibrillary tangle-associated collapsin response mediator protein-2 (CRMP-2) is highly phosphorylated on Thr-509, Ser-518, and Ser-522. Biochemistry 2000; 39: 4267–75.

Harrington EP, Zhao C, Fancy SP, Kaing S, Franklin RJ, Rowitch DH. Oligodendrocyte PTEN is required for myelin and axonal integrity, not remyelination. Ann Neurol 2010; 68: 703–16.

Hellstrom M, Harvey AR. Retinal ganglion cell gene therapy and visual system repair. Curr Gene Ther 2011; 11: 116–31.

Johns TG, Kerlero de Rosbo N, Menon KK, Abo S, Gonzales MF, Bernard CC. Myelin oligodendrocyte glycoprotein induces a demyelinating encephalomyelitis resembling multiple sclerosis. J Immunol 1995; 154: 5536–41.

Jurewicz A, Matysiak M, Raine CS, Selmaj K. Soluble Nogo-A, an inhibitor of axonal regeneration, as a biomarker for multiple sclerosis. Neurology 2007; 68: 283–7.

Karnezis T, Mandemakers W, McQualter JL, Zheng B, Ho PP, Jordan KA, et al. The neurite outgrowth inhibitor Nogo A is involved in autoimmune-mediated demyelination. Nat Neurosci 2004; 7: 736–44.

Kawano Y, Yoshimura T, Tsuboi D, Kawabata S, Kaneko-Kawano T, Shirataki H, et al. CRMP-2 is involved in kinesin-1-dependent transport of the Sra-1/WAVE1 complex and axon formation. Mol Cell Biol 2005; 25: 9920–35.

Kim JE, Liu BP, Park JH, Strittmatter SM. Nogo-66 receptor prevents raphespinal and rubrospinal axon regeneration and limits functional recovery from spinal cord injury. Neuron 2004; 44: 439–51.

Kimura T, Watanabe H, Iwamatsu A, Kaibuchi K. Tubulin and CRMP-2 complex is transported via Kinesin-1. J Neurochem 2005; 93: 1371–82.

Kwon BK, Sekhon LH, Fehlings MG. Emerging repair, regeneration, and translational research advances for spinal cord injury. Spine (Phila Pa 1976) 2010; 35: S263–S270.

Leaver SG, Cui Q, Bernard O, Harvey AR. Cooperative effects of bcl-2 and AAV-mediated expression of CNTF on retinal ganglion cell survival and axonal regeneration in adult transgenic mice. Eur J Neurosci 2006; 24: 3323–32.

Lee JK, Kim JE, Sivula M, Strittmatter SM. Nogo receptor antagonism promotes stroke recovery by enhancing axonal plasticity. J Neurosci 2004; 24: 6209–17.

Li S, Liu BP, Budel S, Li M, Ji B, Walus L, et al. Blockade of Nogo-66, myelin-associated glycoprotein, and oligodendrocyte myelin glycoprotein by soluble Nogo-66 receptor promotes axonal sprouting and recovery after spinal injury. J Neurosci 2004; 24: 10511–20.

Lucchinetti C, Bruck W, Parisi J, Scheithauer B, Rodriguez M, Lassmann H. Heterogeneity of multiple sclerosis lesions: implications for the pathogenesis of demyelination. Ann Neurol 2000; 47: 707–17.

McGee AW, Strittmatter SM. The Nogo-66 receptor: focusing myelin inhibition of axon regeneration. Trends Neurosci 2003; 26: 193–8.

McQualter JL, Darwiche R, Ewing C, Onuki M, Kay TW, Hamilton JA, et al. Granulocyte macrophage colony-stimulating factor: a new putative therapeutic target in multiple sclerosis. J Exp Med 2001; 194: 873–82.

Mi S, Hu B, Hahm K, Luo Y, Kam Hui ES, Yuan Q, et al. LINGO-1 antagonist promotes spinal cord remyelination and axonal integrity in MOG-induced experimental autoimmune encephalomyelitis. Nat Med 2007; 13: 1228–33.

Mimura F, Yamagishi S, Arimura N, Fujitani M, Kubo T, Kaibuchi K, et al. Myelin-associated glycoprotein inhibits microtubule assembly by a Rho-kinase-dependent mechanism. J Biol Chem 2006; 281: 15970–79.

Petratos S, Azari MF, Ozturk E, Papadopoulos R, Bernard CC. Novel therapeutic targets for axonal degeneration in multiple sclerosis. J Neuropathol Exp Neurol 2010; 69: 323–34.

Petratos S, Li QX, George AJ, Hou X, Kerr ML, Unabia SE, et al. The -amyloid protein of Alzheimer's disease increases neuronal CRMP-2 phosphorylation by a Rho-GTP mechanism. Brain 2008; 131: 90–108.

Pool M, Niino M, Rambaldi I, Robson K, Bar-Or A, Fournier AE. Myelin regulates immune cell adhesion and motility. Exp Neurol 2009; 217: 371–7.

Profyris C, Cheema SS, Zang D, Azari MF, Boyle K, Petratos S. Degenerative and regenerative mechanisms governing spinal cord injury. Neurobiol Dis 2004; 15: 415–36.

Satoh J, Onoue H, Arima K, Yamamura T. Nogo-A and nogo receptor expression in demyelinating lesions of multiple sclerosis. J Neuropathol Exp Neurol 2005; 64: 129–38.

Schmidt H, Rathjen FG. Signalling mechanisms regulating axonal branching in vivo. Bioessays 2010; 32: 977–85.

Schnell L, Schwab ME. Axonal regeneration in the rat spinal cord produced by an antibody against myelin-associated neurite growth inhibitors. Nature 1990; 343: 269–72.

Taghian K, Lee JY, Petratos S. Phosphorylation and cleavage of the family of collapsin response mediator proteins may play a central role in neurodegeneration following CNS trauma. J Neurotrauma 2012. Advance Access published on February 29, 2012, doi:10.1089/neu.2011.2063.

Takata K, Kitamura Y, Nakata Y, Matsuoka Y, Tomimoto H, Taniguchi T, et al. Involvement of WAVE accumulation in Abeta/APP pathology-dependent tangle modification in Alzheimer's disease. Am J Pathol 2009; 175: 17–24.

Trapp BD, Peterson J, Ransohoff RM, Rudick R, Mork S, Bo L. Axonal transection in the lesions of multiple sclerosis. N Engl J Med 1998; 338: 278–285.

Wang D, Ayers MM, Catmull DV, Hazelwood LJ, Bernard CC, Orian JM. Astrocyte-associated axonal damage in pre-onset stages of experimental autoimmune encephalomyelitis. Glia 2005; 51: 235–40.

Wang X, Baughman KW, Basso DM, Strittmatter SM. Delayed Nogo receptor therapy improves recovery from spinal cord contusion. Ann Neurol 2006; 60: 540–9.

Williamson R, van Aalten L, Mann DM, Platt B, Plattner F, Bedford L, et al. CRMP2 hyperphosphorylation is characteristic of Alzheimer's disease and not a feature common to other neurodegenerative diseases. J Alzheimers Dis 2011; 27: 615–25.

Yang Y, Liu Y, Wei P, Peng H, Winger R, Hussain RZ, et al. Silencing Nogo-A promotes functional recovery in demyelinating disease. Ann Neurol 2010; 67: 498–507.

Yoshida H, Watanabe A, Ihara Y. Collapsin response mediator protein-2 is associated with neurofibrillary tangles in Alzheimer's disease. J Biol Chem 1998; 273: 9761–8.

Zorner B, Schwab ME. Anti-Nogo on the go: from animal models to a clinical trial. Ann N Y Acad Sci 2010; 1198 (Suppl 1): E22–E34.